Journal of Asian Earth Sciences 70–71 (2013) 142–159

Contents lists available at SciVerse ScienceDirect

Journal of Asian Earth Sciences

journal homepage: www.elsevier.com/locate/jseaes

Compositional variation of the late Cretaceous–Paleogene plutons from southwest Japan and its implication for ore genesis and continental growth

Yuan-Hui Li [a,*], Shunso Ishihara [b]

[a] Department of Oceanography, University of Hawaii at Manoa, Honolulu, HI 96822, USA
[b] Geological Survey of Japan, AIST Central 7, Higashi 1-1-3, Tsukuba 305-8567, Japan

ARTICLE INFO

Article history:
Received 17 June 2011
Received in revised form 21 February 2013
Accepted 18 March 2013
Available online 30 March 2013

Keywords:
Japanese island arc
Subduction zone
Fertile primitive mantle
Primary magma
Factor analysis
xy-Correlation plots
Mafic
Felsic
W–Sn ores
Mo ores
Continental growth

ABSTRACT

During the late Cretaceous–Paleogene period, the fluids liberated from the subducting slab along Japanese-arc subduction zone could have triggered the partial melting of the mantle wedge, whose composition was similar to the fertile primitive mantle. Underplating of the produced basaltic magmas beneath the continental crust could further facilitate the partial melting of the lower continental crusts. The primary magmas produced by the mixing of resultant partial melts underwent various degrees of fractional crystallization processes to produce the late Cretaceous–Paleogene plutons in southwest Japan, and have contributed to the growth of continental crust with new, non-recycled materials during the Phanerozoic.

The factor analysis of chemical data from ore-barren Ryoke and W–Sn-ore-rich Sanyo plutonic rocks identifies three major groups of elements: the mafic group (Al, Fe, Mg, Mn, Ca, Sr, Zn, Co, V, P, Cu, Ni, and Cr); the felsic group (Si, K, Rb, Cs, Tl, Pb, Y, Nb, Ta, Hf, Ge, Sn, W, Th, U, and HREE); and the LREE + Zr group (Ba, La, Ce, Pr, Nd, Eu, Zr, and Hf). Mafic group and felsic group elements are inversely correlated. The concentrations of LREE + Zr group elements increase first, then, decrease with increasing SiO_2 content. Therefore, the high silica samples of the Ryoke + Sanyo belts are low in LREE + Zr group elements. In the Ryoke samples Mo behaves like Zr, which results in the lowest Mo content in the Ryoke samples with high silica. The high Mo and Si contents in some Sanyo samples suggest that the zircon-compatible Mo^{4+} may be converted to incompatible Mo^{6+} under a relatively high oxygen fugacity condition at the late stage of magmatic differentiation. W and Sn behave as the felsic group elements in the Ryoke + Sanyo samples. Thus, their concentrations are high in the high silica granitoids, especially rock samples from the Sanyo belt, which are often associated with W–Sn ores. The factor analysis of the Sanin plutonic samples indicates that W still belongs to the felsic group, but Sn no longer correlates with W and behaves more like Zr due to the conversion of incompatible Sn^{2+} to zircon-compatible Sn^{4+} under a relatively high oxygen fugacity condition in the Sanin belt. Therefore, Sn content is low in high silica granitoids from Sanin belt. The high silica Sanin samples are often enriched in Mo, again suggesting the conversion of zircon-compatible Mo^{4+} into incompatible Mo^{6+} in the magmas of those samples. The high Mo granitoids from the Sanin belt are probable source rocks for the associated Mo ores in the area.

© 2013 Elsevier Ltd. All rights reserved.

1. Introduction

Japanese island arc mainly consists of the late Paleozoic to Cenozoic accretionary complexes, which resulted from the orogens related to the subduction of oceanic crust (Isozaki, 1996; Isozaki et al., 2010). The accretionary complexes contain Precambrian metamorphosed sediments and re-melted crustal materials (Jahn, 2010) and/or other components derived from the partial melts of oceanic crust and upper mantle (Maruyama, 1997; Togashi et al., 2000; Nakajima et al., 2004). The present study focuses on the compositional variation of the late Cretaceous–Paleogene plutons and the related ore formation processes in southwest (SW) Japan.

As shown in Fig. 1, the late Cretaceous–Paleogene plutons from SW Japan (above the Median Tectonic Line) are divided into three major belts: the ore-barren Ryoke belt (110–70 Ma); W–Sn-ore-rich Sanyo belt (110–70 Ma); and Mo-ore-rich Sanin belt (85–30 Ma; Ishihara, 1978). The plutons consist mainly of granite, granodiorite with some quartz diorite, diorite, and gabbro. We loosely call a pluton granitic when $SiO_2 > 52\%$; otherwise, it is considered gabbroic. Plutonic rocks from the Ryoke and Sanyo belts are characterized by their systematically high $\delta^{18}O$ values as compared with those from Sanin belt at a given SiO_2 content (Fig. 2a; data from Ishihara and Matsuhisa, 2002). This is probably an

* Corresponding author. Tel.: +1 808 956 6297; fax: +1 808 956 7112.
E-mail address: yhli@soest.hawaii.edu (Y.-H. Li).

1367-9120/$ - see front matter © 2013 Elsevier Ltd. All rights reserved.
http://dx.doi.org/10.1016/j.jseaes.2013.03.009

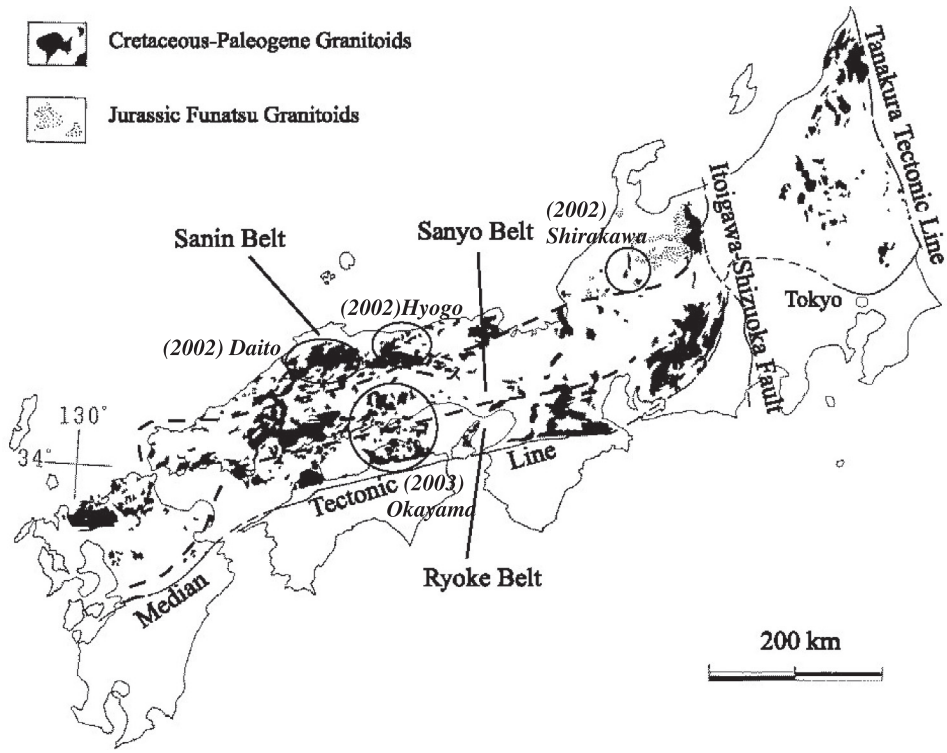

Fig. 1. The areas of Ryoke, Sanyo, and Sanin belts in SW Japan delineated roughly by dashed lines (adopted from Ishihara, 1978).

indication of greater incorporation of continental crust material (with high $\delta^{18}O$ values) for the former than the latter during the formation process of primary magmas. In Fig. 2a, a few samples with very low $\delta^{18}O$ (outside of ovals) may be caused by the exchange with meteoric water. A few Sanin samples fall within the upper oval of Ryoke + Sanyo field and vice versa, indicating some degree of inter-fingering across the belt boundary. The increase in the value of $\delta^{18}O$ with increasing SiO_2 content in each oval may represent the effect of fractional crystallization (removal of mafic minerals with lower $\delta^{18}O$ values causes the residual magma to become higher in $\delta^{18}O$). Sanin samples are mostly high in magnetic susceptibility due to the presence of magnetite ($FeO{\cdot}Fe_2O_3$) and thus are called the magnetite series rocks; Ryoke + Sanyo samples are mostly low in magnetic susceptibility and are called the ilmenite ($FeO{\cdot}TiO_2$) series rocks (Kanaya and Ishihara, 1973; Ishihara, 1977). Sanin rocks were probably formed under higher oxygen fugacity conditions than the Ryoke + Sanyo rocks. The $\delta^{34}S$ values for bulk rocks and sulfide ores from Ryoke + Sanyo belts tend to be more negative (−11‰ to +3‰), while those from Sanin belt are more positive (−2‰ to +10‰; Sasaki and Ishihara, 1979; Ishihara and Sasaki, 2002). The low oxygen fugacity and low $\delta^{34}S$ in Ryoke + Sanyo belts may result from the incorporation of some isotopically light biogenic sulfur and carbon from source rocks of sedimentary origin into their primary magmas (Ishihara and Sasaki, 2002).

The Sr and Nd isotopic ratios for rock samples are often expressed in the initial $^{87}Sr/^{86}Sr$ ratio (I_{Sr}) and the initial $^{143}Nd/^{144}Nd$ ratio (I_{Nd}) at the time of sample formation, and the epsilon notations of ε_{Sr} and ε_{Sr}. For example,

$$I_{Sr} = (^{87}Sr/^{86}Sr)_t = (^{87}Sr/^{86}Sr)_p - (^{87}Rb/^{86}Sr)_p[\exp(\lambda t) - 1]$$

and $\varepsilon_{Sr} = [(^{87}Sr/^{86}Sr)_t/(^{87}Sr/^{86}Sr)_{CHUR,t} - 1] \times 10^4$

Here, t represents the age of sample; p is the present (i.e. $t = 0$); and λ is the decay constant of $^{87}Rb = 1.42 \times 10^{-11}$ year^{-1}. The reference material CHUR is the Chondritic Uniform Reservoir (Faure and Mensing, 2005). For I_{Nd} and ε_{Nd}, one just replaces $^{87}Sr/^{86}Sr$ with $^{143}Nd/^{144}Nd$, $^{87}Rb/^{86}Sr$ with $^{147}Sm/^{144}Nd$ in the above equations, and λ for $^{147}Sm = 6.54 \times 10^{-12}$ year^{-1}.

As shown by Kagami et al. (1992), the majority of the Ryoke + Sanyo samples have narrow ranges in their initial ε_{Sr} and ε_{Nd} values, and those values are almost constant as SiO_2 content increases (the oval RS in Fig. 2b and d), although their formation age varies from 72 to 93 Ma. The implication is that plutonic rocks from the Ryoke + Sanyo belts might evolve from primary magmas that were produced at different times and places from the upper mantle whose composition is rather uniform with regard to $\delta^{18}O$, ε_{Sr}, and ε_{Nd} values in SW Japan. During magmatic differentiation, ε_{Sr}, and ε_{Nd} values stay more or less constant, while $\delta^{18}O$ increases with SiO_2 content through fractional crystallization (Fig. 2a and d). It is hard to produce these features by a simple two-end-member mixing of gabbroic magma (high in ε_{Nd} and low in ε_{Sr} and $\delta^{18}O$) and granitic melt (low in ε_{Nd} and high in ε_{Sr} and $\delta^{18}O$). Nakajima et al. (2004) confirmed that the ε_{Sr} values are near constant (mostly 40–50) as SiO_2 content increases (similar to Fig. 2b) for additional Ryoke plutonic samples (71–86 Ma), including gabbroic cumulates and dykes/pillows, and granites. The close spatial and temporal association of gabbroic and granitic plutons from Ryoke belt points to the importance of magmatic differentiation for their genesis (Nakajima et al., 2004).

The Sanin belt has two distinct primary magmas (the ovals S1 and S2 in Fig. 2b and d). Again, the respective ε_{Sr} and ε_{Nd} values for S1 and S2 are near constant as SiO_2 content increases, suggesting the independent magmatic differentiation for S1 and S2 groups. The formation ages of S1 are around 65 Ma; and of S2 65–75 Ma (Kagami et al. (1992). The ε_{Sr} and ε_{Nd} values for the Sanin rocks, especially the S1 samples, are close to those of the CHUR (Fig. 2c). Samples 26–30 (following the sample assignment by Kagami et al., 1992) are in the transition zone (the oval T in

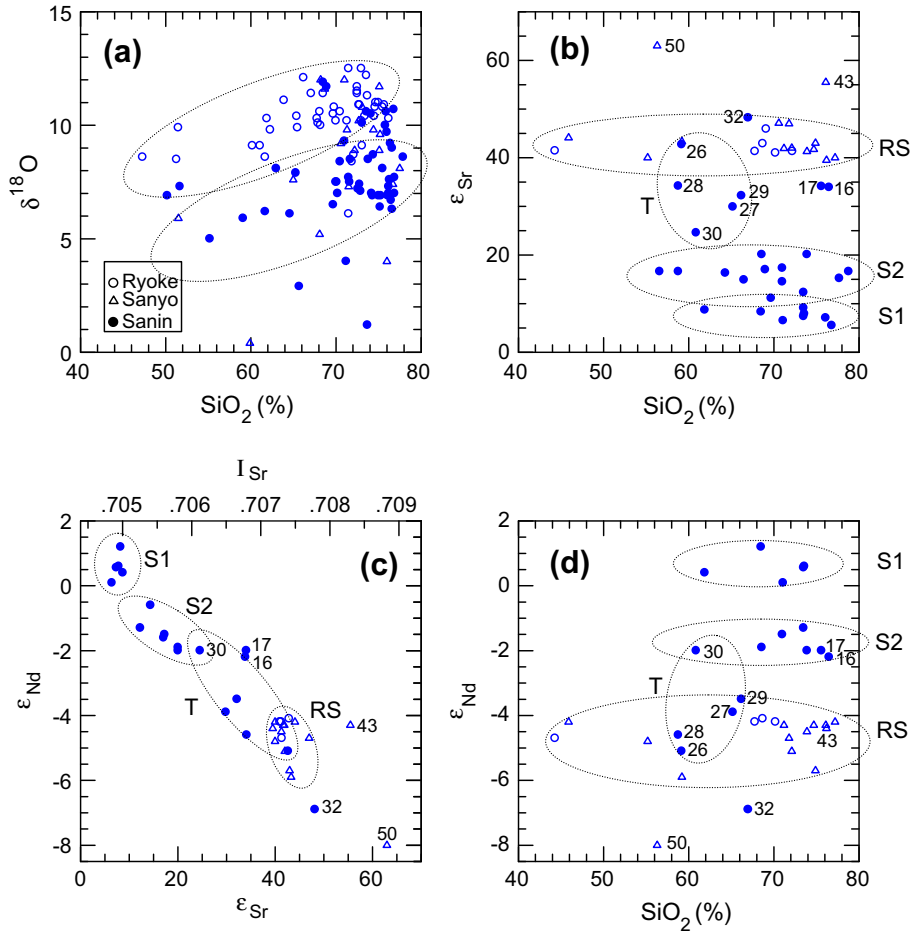

Fig. 2. (a) $\delta^{18}O$ of plutonic rocks from Ryoke (open circle), Sanyo (open triangle), and Sanin (closed circle) belts as a function of SiO_2 content; (b) the initial ε_{Sr} as a function of SiO_2; (c) plot of initial ε_{Sr} versus initial ε_{Nd}. I_{Sr} is the initial $^{87}Sr/^{86}Sr$ ratio; and (d) the initial ε_{Nd} as a function of SiO_2. RS = Ryoke + Sanyo field, S1 and S2 = Sanin field, and T = transition between S2 and RS.

Fig. 2b–d). Their formation age is 72 Ma and their ε_{Sr} and ε_{Nd} values may result from mixing between the RS and S2 reservoirs. Samples outside of ovals (16, 17, 32, 43, and 50 in Fig. 2c) may indicate higher inputs from the continental crust. As surmised by Kagami et al. (1992), the partial melting of the upper mantle and lower continental crust (LCC) with variable proportions produced the primary magmas for the plutons in SW Japan during the Cretaceous–Paleocene period (110–30 Ma).

The fractional crystallization of the primary magmas mainly occurred within magmatic chambers at the boundary between the upper mantle and lower continental crust. The intrusion of magmas into the continental crust at various stages of magmatic differentiation resulted into gabbroic and granitic plutons. After the completion of magmatic differentiation, the volume of resultant mafic cumulates should be an order of magnitude larger than that of granitic plutons (Nakajima et al., 2004). According to Rudnick (1995) and Togashi et al. (2000), a large fraction of those cumulates may have been recycled back to the mantle by the delamination process.

From seismic tomography data, Iwamori (2007), and Kawakatsu and Watada (2007) suggest that water in the subducting oceanic crust and sediments is released at depth shallower than 100 km. Part of released water may convert the peridotitic mantle on top of subducting slab into hydrated serpentine layer. Serpentine layer sinks along with the subducting slab and further release water at depth below 100 km down to 200 km. Basaltic oceanic crust is eventually converted into ecologite with finite water content of about 0.1%, and be transported into the deeper mantle. The released water may percolate upward and facilitate the partial melting of the mantle wedge.

In summary, the plutonic rocks from the Sanin belt and Ryoke + Sanyo belts evolved from different primary magmas, which have distinct isotopic signatures and oxygen fugacity. How the primary magmas might have evolved through fractional crystallization into the ore-barren Ryoke belt, W–Sn-ore rich Sanyo belt, and Mo-ore rich Sanin belt is the focus of the present study. Based on the elemental and isotopic composition data, the probable source rocks for primary magmas are also discussed.

2. Methods and materials

Our approach is to apply the computer program of factor analysis given by the Statistical Package for the Social Sciences (SPSS) to sort out which groups of elements co-vary and which groups of samples are similar or distinct in chemical compositions for a given compositional data matrix. Based on those groupings of elements and samples, a series of *xy*-correlation plots of concentration data for selected elements can be constructed to study in detail the variation patterns of elements among different groups of samples. For the factor analysis, both the principal component and varimax analyses were performed. The details of factor analysis can be found in Davis (1973) and Cooley and Lohnes (1971).

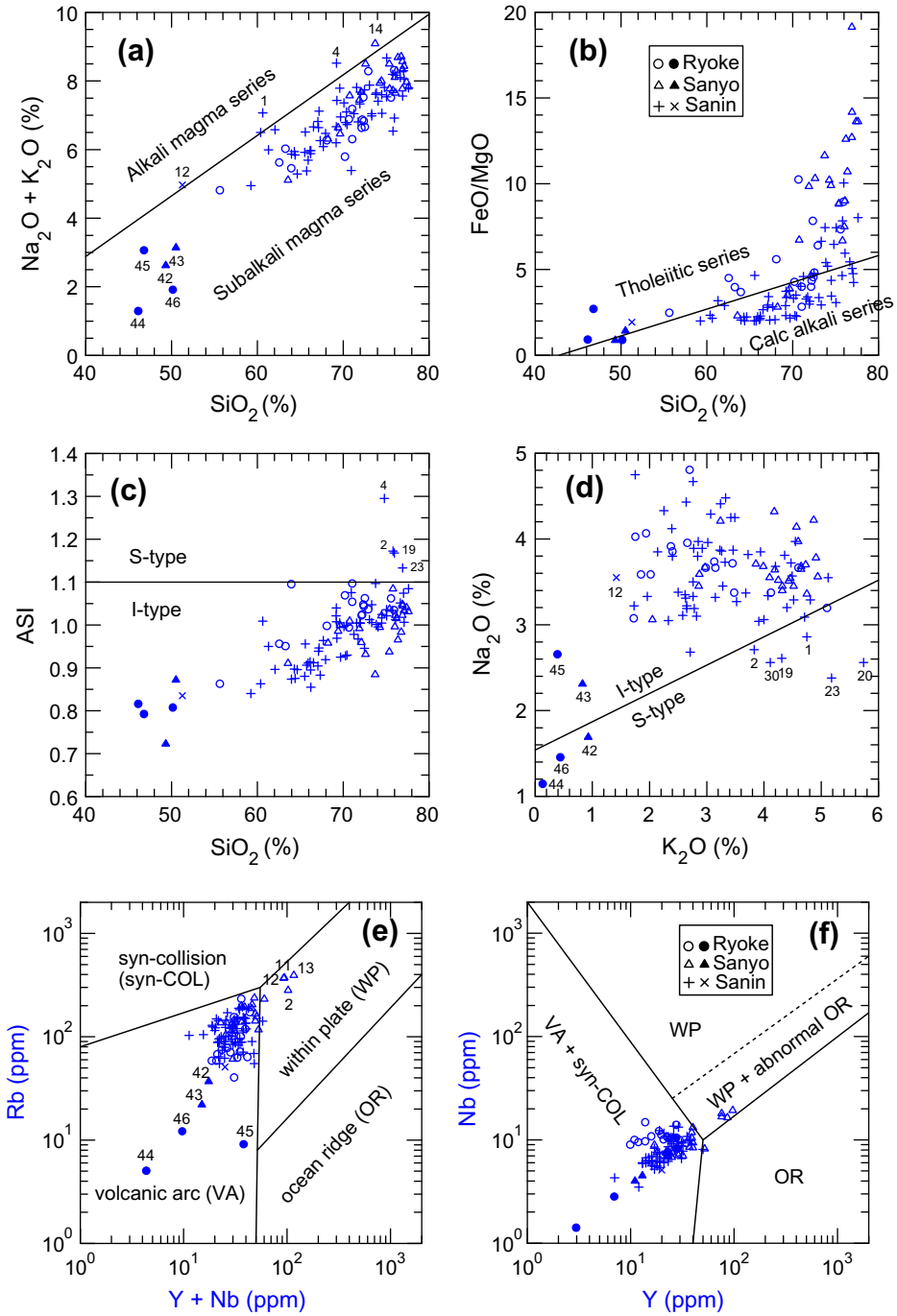

Fig. 3. Rock classification schemes: (a) The total alkali silica (TAS) diagram to distinguish the alkali and subalkali magma series; (b) Miyashiro diagram to subdivide the subalkali magma series into the calc-alkali and tholeiitic series; (c and d) Chappell and White diagrams to separate granitoids into I- (igneous source) and S- (sedimentary source) type; (e and f) Pearce's discrimination diagrams to separate granites into syn-collision, volcanic arc, oceanic ridge, and within plate; (g and h) Discrimination diagrams for separating the island arc adakites from non-adakites (Drummond and Defant, 1990). The dotted vertical line is the possible upper bound of Y or Yb content for adakites. Sample symbols: open circle, open triangle, and plus sign are granitic rocks; and solid circle, solid triangle, and cross are gabbroic samples.

Here we present either the principal component or varimax result, depending on which one gives a clearer presentation of the data set. Useful outputs of SPSS include means and standard deviations of variables, correlation coefficient matrix, eigenvalues, communalities, factor loadings of variables on new factors (proxy correlation coefficient), and factor scores (proxy concentrations) of new factors for each sample.

We selected the compositional data for the Ryoke + Sanyo belt rocks from Ishihara (2003) and Sanin belt rocks from Ishihara (2002a, 2002b) for the present study. Samples were mainly analyzed by Bruce Campbell at Macquarie University, Australia, using the polarized XRF spectrometer (Heckel and Ryon, 2002). All sample identification numbers in the following sections are the same as given by Ishihara (2002a, 2002b, 2003). Details on the sample description and geological setting can be found in the same references.

3. Classification of rock samples

To place our chosen data in a global context, the following rock classification schemes are adopted. The total alkali silica (TAS) diagram in Fig. 3a shows that almost all the samples belong to the

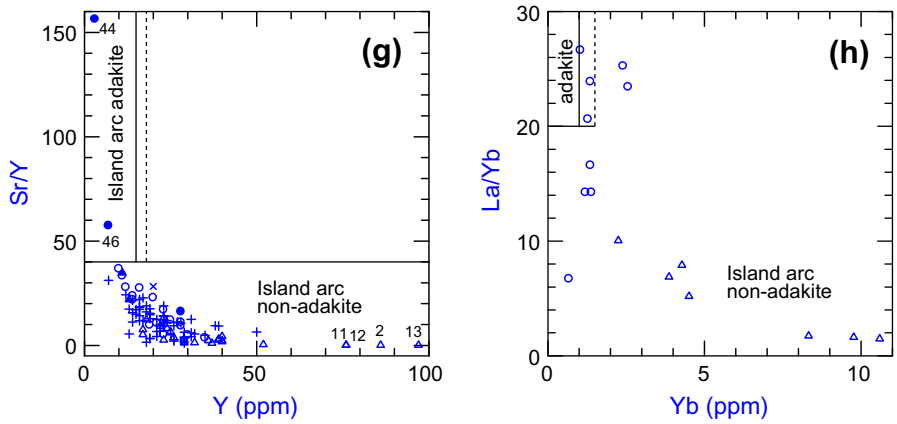

Fig. 3. (*continued*)

sub-alkali magma series except samples 1 and 4 from Sanin and 14 from Sanyo, which fall on the field of alkali magma series. Samples 42–46 and 12 are gabbroic in composition ($SiO_2 \leqslant 52\%$). Per Miyashiro (1974), the sub-alkali magma series can be subdivided into two: the iron depleted calc-alkali series when $SiO_2 > 6.4 \times (FeO/MgO) + 42.8$; otherwise the tholeiitic series. Here all oxides are in weight% and the total Fe is expressed as FeO. As shown in Fig. 3b, the Sanin samples tend to fall more on the calc-alkali series field, and the Ryoke + Sanyo samples on the tholeiitic series field. However, there are many overlaps.

Chappell and White (1974, 2001) separated the granitic batholiths (or granitoids) of the Tasman Orogenic Zone of eastern Australia into two types: I-type (mainly igneous sources) and S-type (mainly sedimentary sources). If $Al_2O_3/(CaO + Na_2O + K_2O) > 1.1$, then S-type; otherwise I-type. Oxides in the above formula are all in units of moles per mass. This ratio is also called the aluminum saturation index (ASI). In addition, if Na_2O (%) $< 0.33 \times K_2O$ (%) + 1.53, then S-type; otherwise I-type. As shown in Fig. 3c and d, most of the granitic samples fall on the I-type field. Only samples 2, 19, and 23 are S-type according to both criteria. This classification scheme only applies to granitic plutons but gabbroic samples 42–46 and 12 are also shown in Fig. 3c and d for reference.

According to the discrimination diagrams proposed by Pearce et al. (1984), granitic samples mostly fall on the volcanic arc granite (VAG) field (Fig. 3e and f), as also shown by Kagami et al. (1992). A few exceptions (samples 2, 11, 12, and 13) are leucogranites (or aplite). As discussed later, those leucogranites may not necessarily belong to the within-plate granite (WPG). No sample falls on the ocean-ridge granite (ORG) field. Again, the gabbroic samples are shown in Fig. 3e and f just for reference.

Igneous rocks formed mainly by the melting of subducting oceanic crust are called the island arc adakites (Drummond and Defant, 1990); and are characterized by the high Sr/Y (>40) and La/Yb (>20) weight ratios, and low Y and Yb contents (15–18 ppm Y and 1–1.5 ppm Yb). As shown in Fig. 3g and h, all granitic samples from SW Japan fall outside of the field of island arc adakites, i.e. non-adakites. Therefore, the contribution of subducted oceanic crust to our selected granitic samples is probably negligible. The Ryoke gabbroic samples 44 and 46 fall on the field of adakites (Fig. 3g), but as discussed later they are actually cumulates with high contents of plagioclase and hornblende. So far there is only one formal report on the occurrence of adakites in Sanyo belt (Kiji et al., 2000). In short, our selected granitoid samples from SW Japan predominantly belong to the class of sub-alkali, I-type, volcanic-arc, and non-adakite granites. This is confirmed by additional data given by Ishihara and Chappell (2007, 2008).

4. Results and discussion

4.1. Chemical characteristics of rocks from ore-barren Ryoke belt and W–Sn-ore-rich Sanyo belt

Chemical data of 47 samples from the Ryoke and Sanyo belts around Okayama–Kagawa Prefectures (Ishihara, 2003) were chosen for factor analysis. All concentration data in the format of "less than x" are replaced by the value of $x/2$. Data for S, H_2O^+, C, As, Se, Mo, Cd, Ta, and Bi are excluded in the final factor analysis because those variables do not correlate highly (correlation coefficient $\gamma < 0.5$) with one another nor with other elements. In addition, the concentrations of S, As, Se, Cd, Ta, and Bi are close to the analytical detection limits in many cases, thus they have large analytical uncertainties. However, some of those elements are discussed whenever they are relevant.

Three factors with eigenvalue greater than 1 were extracted from the Ryoke + Sanyo data set and these three factors can explain 79% of the total variance (factor 1, 50%; factor 2, 19%; and factor 3, 10%). The factor loading data are plotted in Fig. 4a and b. However, some elements with factor loadings of less than 0.5 for both plotted factors are not shown. Elements within any dotted oval in Fig. 4a have the correlation coefficient (γ) of equal to or greater than 0.5 among all pairs. The positive factor 1 (F1) consists of Si, K, Rb, Cs, Tl, Pb, Y, Ge, Sn, W, Th, and U; Hf and Na are partially related to F1 through Si and K. Hereafter, those elements will be referred to as the felsic group elements. The negative factor 1 (−F1) consists mainly of two ovals: one comprises Al, Fe, Mn, Ca, Sr, Zn and P; and the other Al, Fe, Mn, Ca, Mg, Co, V, Cu, Ni, and Cr. These two ovals are closely related through the common elements Al, Fe, Mn, and Ca. The positive factor 2 (F2) represents Ni and Cr. All those elements are referred to as the mafic group elements (−F1 and F2) hereafter. The negative factor 2 (−F2) includes La, Ce, Zr, and Ba; Hf and Na are partially related to −F2 through La and Ce. The positive factor 3 (F3) consists of Nb, Y, Ga, and P (Fig. 4b). However, Nb and Y are also closely related to F1; and Ga and P with −F1 through Ti and Zn, as evident in Fig. 4a. The correlation matrix obtained among rare earth elements (REE), Rb, Sr, Ba, Y, Th, and U for 13 selected samples from the Ryoke and Sanyo belts (Table 3 of Ishihara, 2003) further indicates that Pr, Nd, and Eu belong to the −F2 group (La, Ce, Zr, and Ba); and Sm, Gd, and other heavy REE belong to the F1 group (felsic group elements). Hereafter, the −F2 group is called the LREE + Zr group. The elements As, Ta, and Bi tend to have high concentrations for a few high silica samples, thus may also belong to the felsic (F1) group elements.

The factor score results are shown in Fig. 4c and d. The Sanyo samples are shown as open triangles (gabbroic), open circles

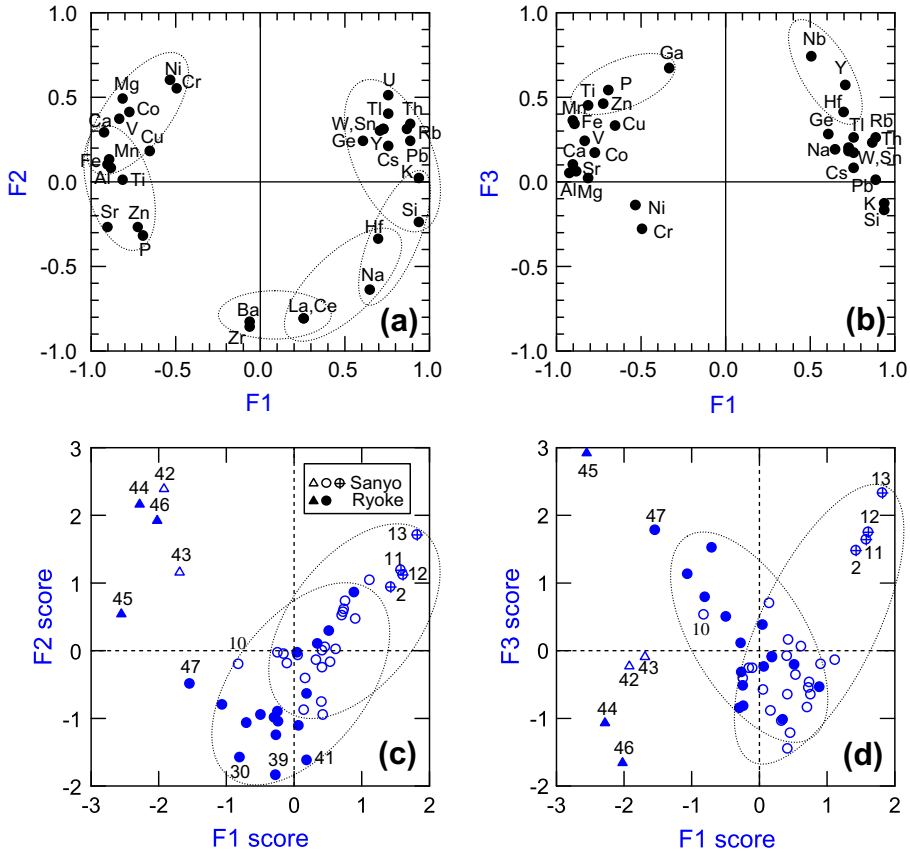

Fig. 4. (a and b) Plots of three extracted factor loadings for Ryoke + Sanyo belt data. Elements within any dotted oval have the correlation coefficient of equal to or greater than 0.5 among all pairs; (c and d) plots of factor scores. Sample symbols: open triangle = gabbroic, open circle = granitic, and open circle with plus = leucogranite for Sanyo; solid triangle = gabbroic, solid triangle = granitic for Ryoke. Numerals are sample labels according to Ishihara (2003).

(granitic), and open circles with cross (unusual leucogranite). The Ryoke samples are shown as solid triangles (gabbroic) and solid circles (granitic). Gabbroic samples 42–46 (open and solid triangles) are mostly high in the mafic group elements (−F1 and F2 elements), especially gabbroic samples 42, 43, 44, and 46, which are also high in Ni and Cr (F2 elements) and low in Ga and P (F3 elements) when compared to gabbroic sample 45. The Ryoke granitic samples are mostly high in LREE + Zr group elements (−F2) (Fig. 4c). The Sanyo granitic samples are mostly high in the felsic group elements (F1), especially the leucogranite samples (2, 11, 12, 13), which are also high in Y and Nb (Fig. 4d) as well as Hf and Ta (not shown). Excluding gabbroic samples 42–46 and Sanyo sample 10, the fields occupied by the Ryoke and Sanyo granitic samples in Fig. 4c and d (dotted ovals) do overlap somewhat.

The best way to explain the observed variation patterns shown in Fig. 4 is the fractional crystallization of basaltic primary magmas, which were in turn produced by the partial melting of upper mantle and lower continental crust. In an island arc or continental arc setting, the partial melting of the mantle wedge may be facilitated by the fluids liberated from a subducting oceanic crust and sediments (Kessel et al., 2005a,b; Spandler et al., 2007; Iwamori, 2007; Kawakatsu and Watada, 2007). Gabbroic sample 45 may represent the overall primary magma composition in this area. The first batch of minerals crystallized and settled from the primary magmas should contain the mafic group elements, next the LREE + Zr group, and finally Na-feldspar. The residual magmas are concentrated in the felsic group elements. As discussed later, the gabbroic samples 42, 43, 44, and 46 may represent cumulates formed at the early stage of magmatic differentiation.

If the composition of mantle wedge under the SW Japan is relatively homogeneous, and the degree of partial melting of mantle wedge and the fraction of continental crust contribution to the primary magmas are all similar (which are probable when all primary magmas were formed under similar physical conditions), then the composition of primary magmas for the Ryoke + Sanyo samples would be all similar regardless of time and space. Each sample, which was emplaced in the crust, represents a snapshot of a certain degree of fractional crystallization for a given primary magma chamber. Therefore, when putting all the samples together, it is possible to discern the magmatic differentiation through fractional crystallization in the whole sampling area during the last 70–110 Ma.

Factor analysis provides only the overall correlation patterns among elements and samples. For more a detailed picture, it is necessary to look back at the original raw data. Figs. 5–7 provide the *xy*-correlation plots for the concentrations of selected mafic (−F1 and F2), LREE + Zr (−F2), and felsic (F1) group elements that illustrate in detail the variation patterns of elements among different sample groups during magmatic differentiation, and provide a possible explanation for the changing patterns. For reference, the average composition of continental basalts (Li, 2000) is also plotted in those figures as an open star symbol labeled by B.

As shown in Fig. 5, the element noted in a small box on some diagrams has the variation pattern similar to that of the element shown in the *y*-axis. For example, in Fig. 5b, the elements Mn and V have a similar variation pattern as Fe_2O_3. The similarity of the ionic radius among those elements (Fe^{2+} = 0.78, Mn^{2+} = 0.83, and V^{2+} = 0.79 Å) indicates the easy substitution of Fe by Mn and V. It is evident from Fig. 5a–c that gabbroic sample 45 may represent the overall composition of primary magma for the Ryoke + Sanyo belts. The contents of mafic group elements Mg, Co, Fe, Mn, V, P, Ti, Zn, Ga, Al, and Sr in gabbroic sample 45 are

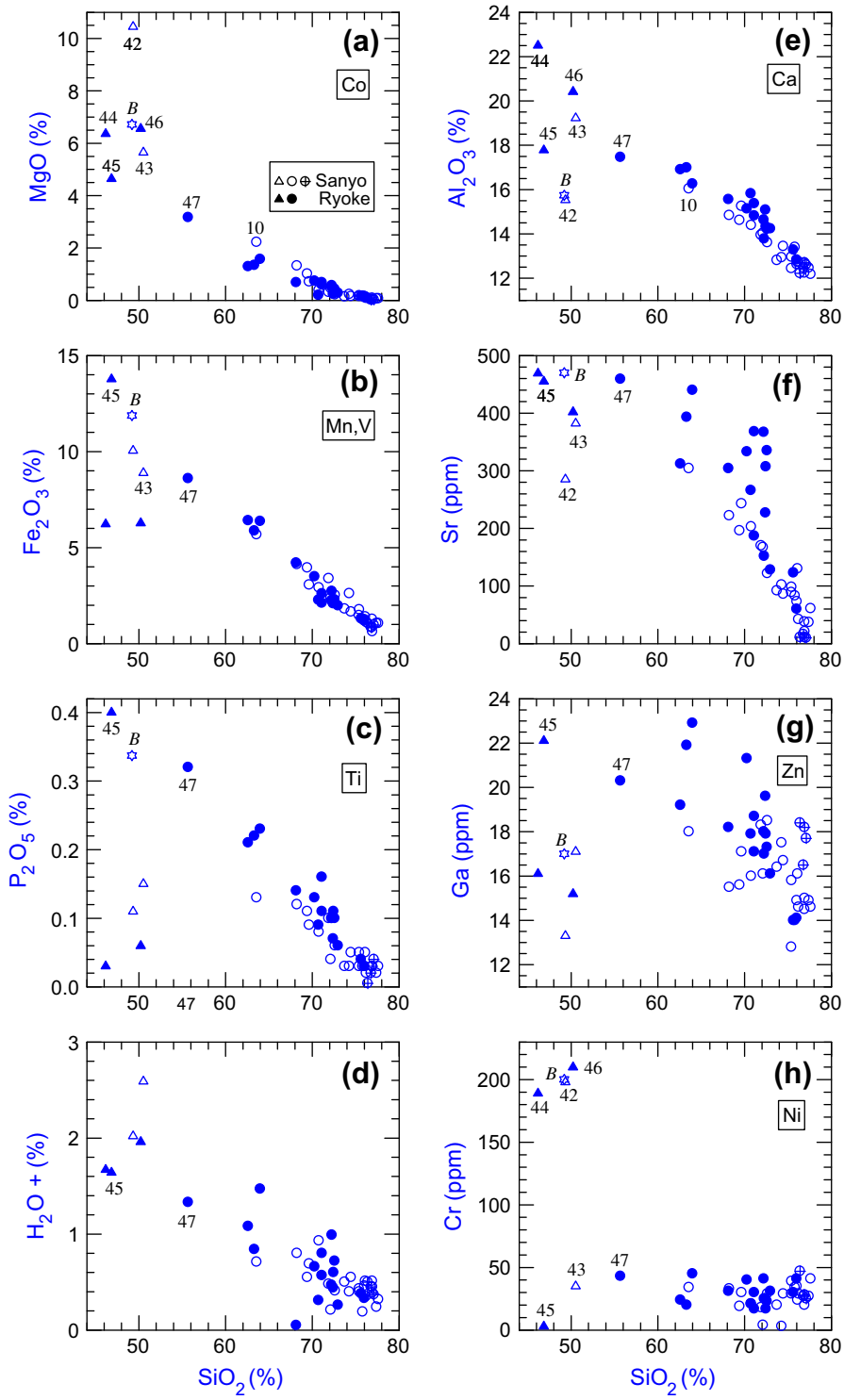

Fig. 5. *XY*-plots of the concentration data among selected mafic group elements and SiO_2 (Ryoke + Sanyo belts). The element noted in a small box on some diagrams has the variation pattern similar to that of the element shown in the *y*-axis. Sample symbols are the same as Fig. 4, except open star with label B = concentration of the given element for the average continental basalts.

similar to those of the world's average basalts (see Fig. 5a–f). However, Cr, Ni, and Cu are much depleted in gabbroic sample 45 (Fig. 5h; Cu data are not shown).

The first batch of minerals crystallized and settled from primary magmas should contain Mg, Co, Cr, and Ni such as garnet $Mg_3Al_2Si_3O_{12}$, chromite $FeCr_2O_4$, nichromite $(Ni,Fe,Co)Cr_2O_4$, and olivine $MgSiO_4$. The next batch could be ilmenite $FeTiO_3$, titanite $CaTiSiO_5$, anorthite $CaAl_2Si_2O_8$, hornblende, biotite, apatite $Ca_5(PO_4)_3(OH,F)$ etc., which contain the other mafic group elements. Gabbroic samples 42, 43, 44, 46 tend to be high in Mg, Co, Cr, Ni, Al, and Ca, but low in Fe, P, Ti, Zn, Ga, and Cu, as compared with sample 45 (Fig. 5). Therefore, those gabbroic samples are probably cumulates at the early stage of magmatic differentiation. According to Nakajima et al. (2004), gabbroic cumulates in Ryoke belt occur as isolated kilometer-size bodies within the massive granitic plutons, and coarse-grained plagioclase and hornblende tend

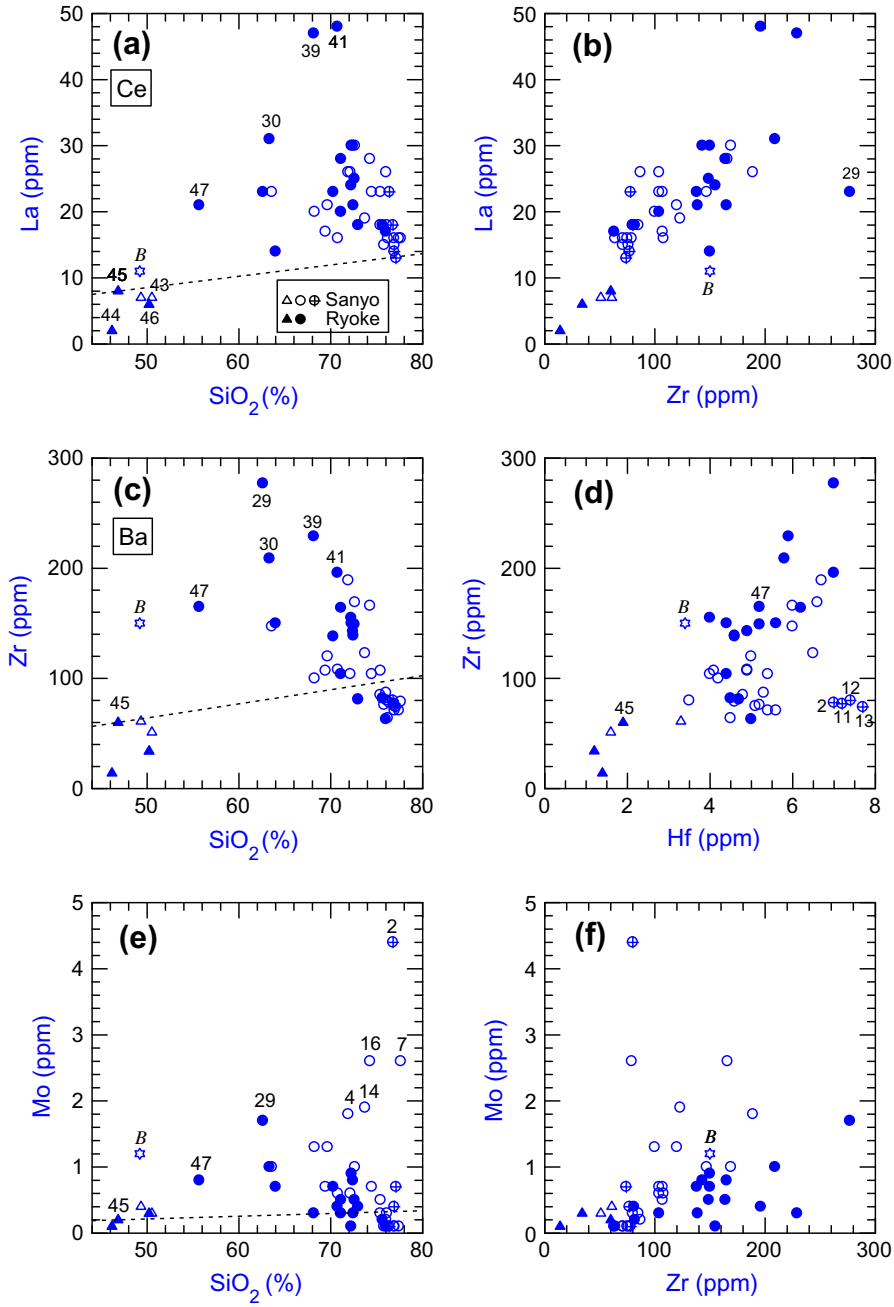

Fig. 6. *XY*-plots of the concentration data among the LREE + Zr group elements and SiO_2 (Ryoke + Sanyo belts). The dotted straight line in each diagram represents the line connecting the origin and the data point of gabbroic sample 45 (primary magma). Symbols are the same as in Figs. 4 and 5.

to form small scale layering. The steady decrease in the concentration of the mafic group elements from gabbroic sample 45 to granitic samples (as SiO_2 content increases) may indicate a steady removal of mafic minerals throughout magmatic differentiation. The crystal lattice water (H_2O^+) content also decreases with increasing SiO_2 content (Fig. 5d), indicating either removal of water by hydrous mafic minerals in dry magmas or reflecting the decrease of water solubility due to a decrease in temperature and pressure during a magmatic differentiation involving water phase.

Variation patterns of the LREE + Zr group elements along with Mo are summarized in Fig. 6. The dotted straight lines in diagrams 6a, 6c, and 6e represent the line connecting the origin and the data point of gabbroic sample 45 (primary magma). A data point above the dotted line means $(X/Si)_{sample} > (X/Si)_{\#45}$ for the chosen element X, and the sample proportionally gains more X than SiO_2 during magmatic differentiation. Below the dotted line [i.e., $(X/Si)_{sample} < (X/Si)_{\#45}$], the sample proportionally gains less X than SiO_2 when $X_{sample} > X_{\#45}$. This also implies that the crystallizing minerals proportionally remove X more than SiO_2. If $X_{sample} < X_{\#45}$, the sample has a net loss of X from magma by the fractional crystallization, which is the case for all mafic group elements (Fig. 5).

For granitic samples, La data points all fall above the dotted line (Fig. 6a). In contrast, the Zr data points at the high end of SiO_2 fall below the dotted line, but $Zr_{sample} > Zr_{\#45}$ (Fig. 6c). The concentrations of La and Zr increase first, and then decrease with increasing SiO_2 (Fig. 6a and c). Therefore, both La and Zr are incompatible elements at the early stage and became compatible at the late stage of magmatic differentiation. The Zr maximum tends to occur earlier

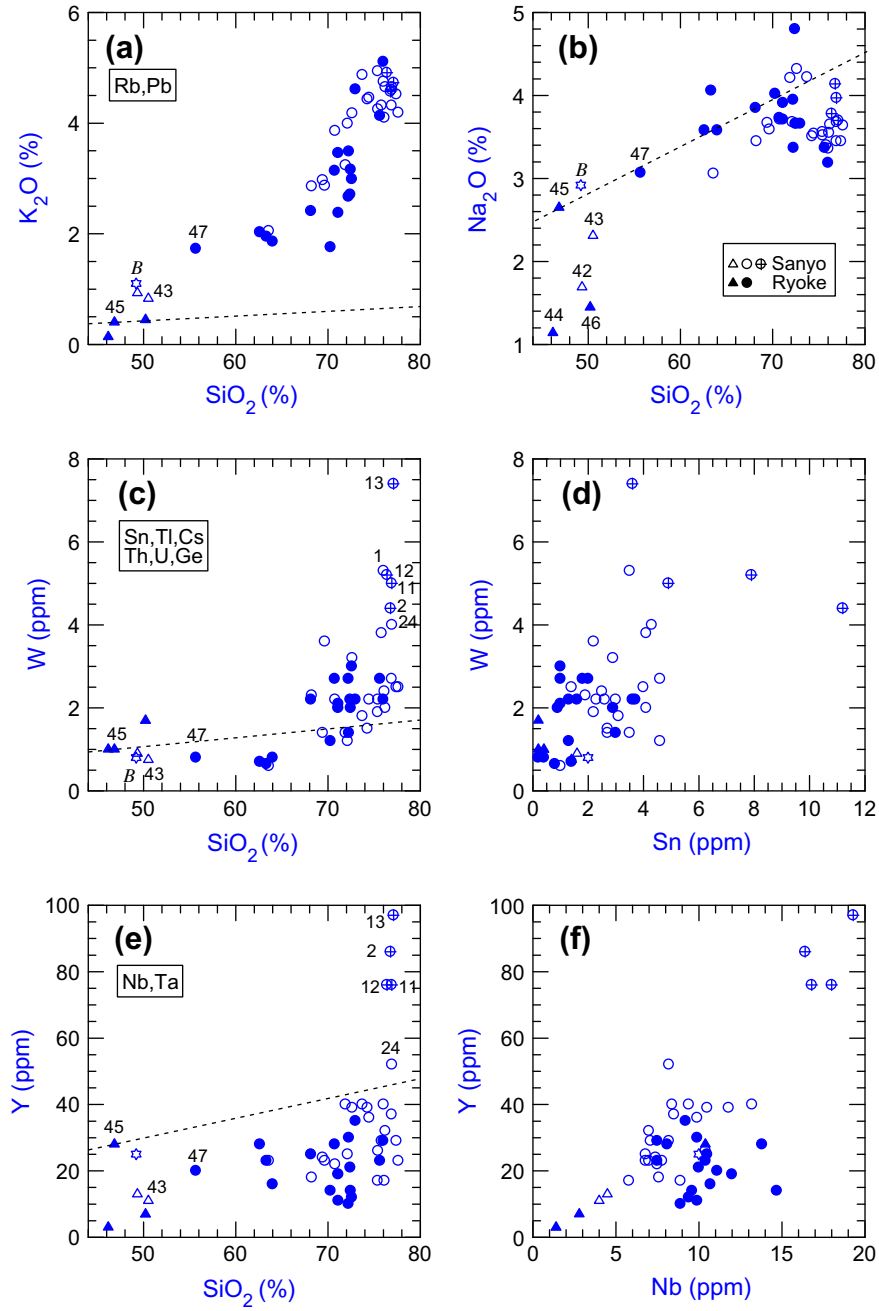

Fig. 7. *XY*-plots of the concentration data among selected felsic group elements and SiO_2 (Ryoke + Sanyo belts). The dotted straight line in each diagram represents the line connecting the origin and the data point of gabbroic sample 45 (primary magma). Symbols are the same as Figs. 4 and 5.

than La maximum, indicating earlier zircon $ZrSiO_4$ removal. La and Ce were probably removed by minerals such as monazite $(La,Ce,Th)PO_4$, apatite, and allanite $(Ca,Ce,La,Y)_2(Al,Fe)_3(SiO_4)_3(OH)$. Those minerals are common in the studied areas (Ishihara, 2002a, 2002b, 2003; Ishihara and Chappell, 2007). Fig. 6b confirms the linear relationship between La and Zr. The Zr/Hf ratio tends to decrease from Ryoke to Sanyo and to Sanyo leucogranite samples (Fig. 6d). As demonstrated by Linnen and Keppler (2002), the Zr/Hf ratio decreases with the progression of magmatic differentiation in aluminous magmas. Excluding the high Mo samples 2, 7, 16, 14, and 4 from the Sanyo belt, Mo concentration also increases with SiO_2 up to a broad maximum around 62% SiO_2, decreases afterward, and then falls below the dotted line (Fig. 6e). By excluding samples 2 and 7 in Fig. 6f, Mo and Zr become highly correlated, and the Sanyo samples tend to have higher Mo/Zr ratio than Ryoke samples. Mo in the ilmenite series magmas may exist as a tetravalent Mo^{4+} and its ionic radius (0.65 Å) is close to Zr^{4+} (0.72 Å). Therefore, Mo can easily fit into the zircon crystal lattice. A study on the distribution coefficient of Mo in a zircon/matrix system will be useful to verify this hypothesis. The high Mo and Si contents in the Sanyo samples 2, 7, 16, 14, and 4 (Fig. 6e) may suggest that the zircon-compatible Mo^{4+} is converted into incompatible Mo^{6+} in the relatively high oxygen fugacity magmas of those samples. Mo ores often occur as molybdenite-quartz vein in granite and sericitized ignimbrites, or as disseminated molybdenite in chloritized granite in the Sanyo belt (Ishihara and Sasaki, 2002). The hydrothermal solutions containing ligands such as halide ions could be important agents for extracting and mobilizing Mo from the plutonic rocks.

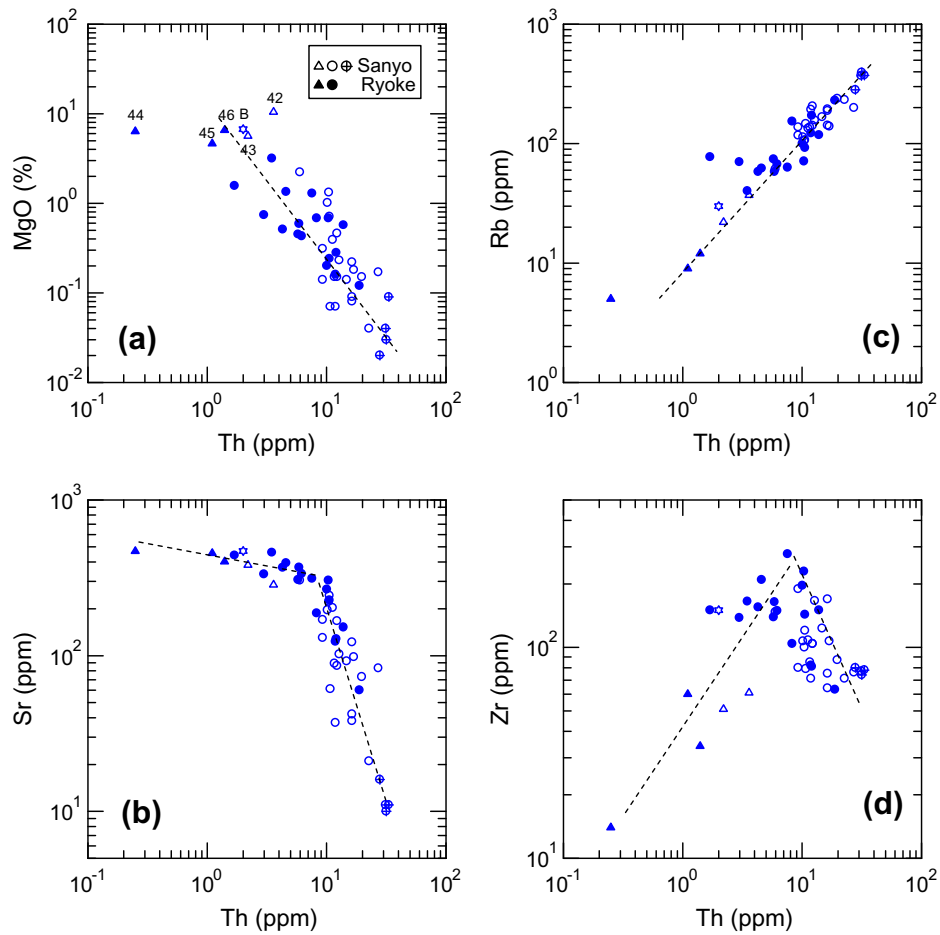

Fig. 8. The plots of logarithmic concentration of Th versus that of (a) Mg, (b) Sr, (c) Rb, and (d) Zr for samples from Ryoke and Sanyo belts. Sample symbols are the same as Fig. 4, except the star with label B = concentration of the given element for the average continental basalts.

The selected felsic group elements are plotted in Fig. 7. The dotted straight line again represents the line connecting the origin and the data point of gabbroic sample 45 (primary magma). The data points for elements K, Rb, and Pb all fall above the dotted line, thus, all samples proportionally gain more K, Rb, and Pb than SiO_2 (Fig. 7a). Most of the Sanyo and Ryoke samples accumulate W (as well as Sn, Tl, Cs, Th, U, and Ge; Fig. 7c) more efficiently than SiO_2. However, some samples are below the dotted line and a few are even $W_{sample} < W_{\#45}$, indicating some removal of W from magma during the early stage of magmatic differentiation, most likely through substitution in mafic minerals. Fig. 7d confirms the general positive correlation between W and Sn, and the Sanyo samples tend to have higher W and Sn contents than the Ryoke. Sn probably exists as divalent Sn^{2+} in the relatively reducing magmas of the Ryoke + Sanyo belts and behaves like an incompatible ion. Data points for Y (Fig. 7e) fall mostly below the dotted line, except for leucogranite samples (2, 11, 12, and 13) and sample 24. The majority of the Ryoke samples have Y content less than gabbroic sample 45. Fig. 7f confirms the positive correlation between Y and Nb. However, the Y/Nb ratio tends to be lower for Ryoke than for Sanyo samples. Y and Nb were probably removed by identified minerals such as monazite, allanite, xenotime YPO_4 in the studied area (Ishihara, 2002a, 2002b, 2003; Ishihara and Chappell, 2007) and even samarskite $(Y,Fe,U)(Nb,Ta)O_4$. The high Y and Nb content in the leucogranite samples may result from the entrapment of those cumulate minerals at the near end of magmatic differentiation. The Na/Si ratio does not change much in the early stage of magmatic differentiation, but Na tends to be removed when SiO_2 became greater than 68% (Fig. 7b) due to the fractional crystallization of Na-feldspar.

The most fractionated residual magma is very much concentrated in the felsic group elements, and may evolve into pegmatite with many rare accessory minerals such as coffinite $U(SiO_4)_{0.9}(OH)_{0.4}$, thorite $ThSiO_4$, yttrialite $(Y,Th)_2Si_2O_7$, columbite $(Fe,Mn)(Nb,Ta)_2O_6$, smarskite, cassiterite SnO_2, wolframite $(Fe,Mn)WO_4$, and scheelite $CaWO_4$. It may even evolve into aplite dykes/veins, cassiterite bearing wolframite-quartz veins, and greisen type Sn–W ores with high F and Li content in the Sanyo belt (Ishihara, 2002a). Urabe (1985) also demonstrated in the laboratory that chlorine-rich hydrothermal solutions can easily leach out Pb and Zn from aluminous granites. Pb–Zn, W–Sn, and U–Th ores are commonly found in the Sanyo Belt.

When a magmatic differentiation follows the Rayleigh fractional crystallization model, a plot of the observed logarithmic concentrations of the element Th versus X (any element other than Th) in magma follows more or less the following relationship:

$$\log X = \left(\log X^0 - \frac{D_X - 1}{D_{Th} - 1}\log Th^0\right) + \frac{D_X - 1}{D_{Th} - 1}\log Th$$
$$= a_1 + a_2 \times \log Th$$

where X^0 and Th^0 represent the initial or time-zero concentrations; D_X and D_{Th} are the bulk distribution coefficients of elements X and Th; and a_1 and a_2 are constants (e.g. Li, 2000). Fig. 8a–d show some examples of this linear relationship. For Mg and Sr (mafic group elements), the slope a_2 are negative, thus D_{Mg} and $D_{Sr} > 1$ (compatible)

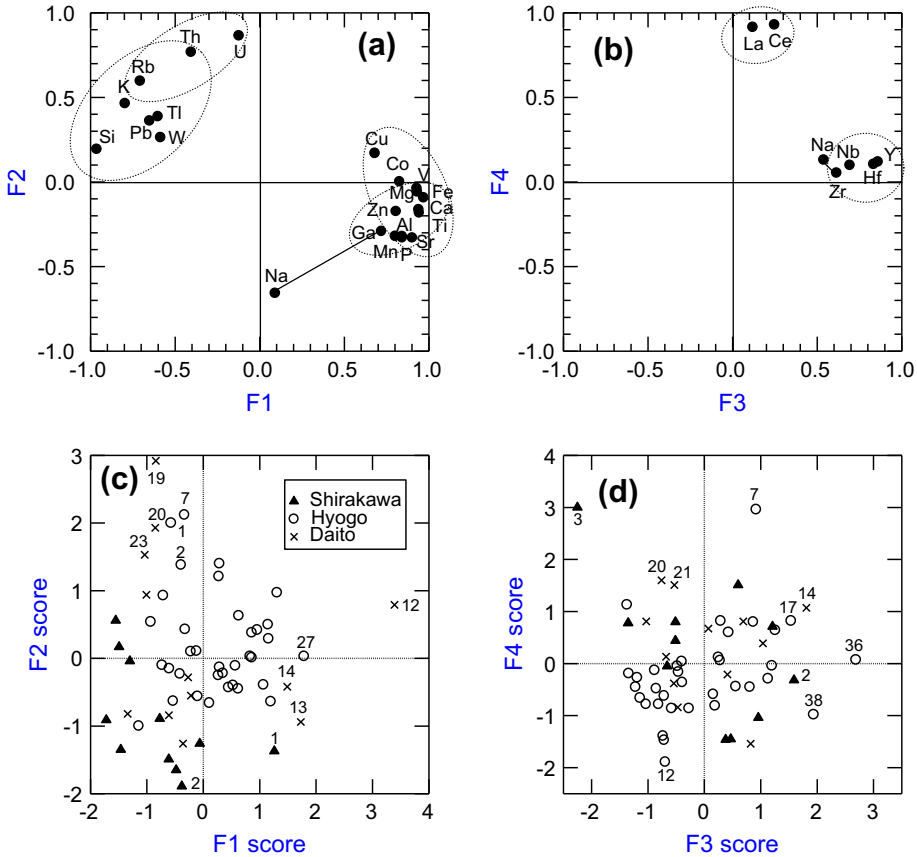

Fig. 9. (a and b) Plots of four extracted factor loadings for Sanin belt data. Elements within any dotted oval have the correlation coefficient of equal to or greater than 0.5 among all pairs; and (c and d) Plots of factor scores. Sample symbols: solid triangle = Shirakawa, open circle = Hyogo, and cross = Daito region. Numerals are sample labels according to Ishihara (2002a, 2002b).

because D_{Th} is a small positive value much less than one. For Rb (felsic group elements), the slope is positive, thus $D_{Rb} < 1$ (incompatible). For Zr (REE + Zr group elements), the slope a_2 is positive at the early stage and shift to negative at the later stage of magmatic differentiation.

4.2. Chemical characteristics of rocks from the Mo-ore-rich Sanin belt

Chemical data for the Sanin belt rocks are selected from the Shirikawa and Daito regions (Ishihara, 2002a) and the Hyogo region (Ishihara, 2002b). Those regions are shown in Fig. 1. Even though the Hyogo samples 1–7 have low magnetic susceptibility, their chemistry is similar to other samples with high magnetic susceptibility. Therefore, they are not distinguished separately here. Samples 4, 18, and 30 from Hyogo are not included in the factor analysis because they were highly metamorphosed (Ishihara, 2002a, 2002b). Unusually high contents of Mo in Shirakawa sample 10 (330 ppm) and Daito sample 17 (32 ppm), and Sn and W in Hyogo sample 5 (5.6 and 76 ppm respectively) are replaced with respective mean values during the factor analysis run. Those high values probably represent inputs from localized mineralization, and are excluded from further discussion. Again all concentration data in the format of "less than x" are replaced by the value of x/2. The elements S, C Cs, Ba, Ge, As, Se, Mo, Sn, Cd, Sb, and Bi do not correlate highly with one another nor with other elements, therefore those elements were not included in the final factor analysis run.

Four factors with eigenvalue greater than 1 (from varimax) were extracted from the Sanin data set and those four factors can explain 81% of the total variance (factor 1, 48%; factor 2, 13%; factor 3, 12%; and factor 4, 8%). Five distinctive groups of elements can be seen in Fig. 9a and b: the mafic group (F1) –Al, Ca, Co, Cu, Fe, Ga, Mg, Mn, P, Sr, Ti, V, Zn; the felsic group (−F1 and F2) – Si, K, Rb, Tl, Pb, W, U, and Th; the Y + Zr group (F3) – Y, Nb, Hf, and Zr; the LREE group (F4) – La and Ce; and Na, which is partially correlated with both Zr (F3) and Ga (F1). The major difference between Sanin and Ryoke + Sanyo results are: Cr and Ni no longer belong to the mafic group elements in Sanin belt, nor Y to the felsic group; the LREE + Zr group in Ryoke + Sanyo belts now split into two independent Y + Zr group and LREE group in the Sanin belt; the close association between Sn and W in Ryoke + Sanyo belts breaks down in the Sanin belt; and Mo and Zr are no longer correlated in the Sanin belt samples.

The concentration data of selected mafic group elements as well as Cr and Ni are plotted in Fig. 10. The gabbroic sample 12 from Daito area may represent the overall primary magma composition for the Sanin belt. Fig. 10a–d all indicate a steady decrease in the concentrations of mafic group elements as the concentration of SiO_2 increases due to the fractional crystallization of mafic minerals. Cr content is high for Shirakawa samples 6, 9, and 10; and Daito samples 15 and 21; which are all high in SiO_2 content (>69%; Fig. 10e). It is possible that the highly compatible Cr^{3+} were converted into incompatible Cr^{6+} for those samples under relatively high oxygen fugacity conditions at the late stage of magmatic differentiation in the Sanin belt. Ni tends to change independently from Cr, except for samples 6 and 10 (Fig. 10f).

The distinct variation patterns of the LREE group and Y + Zr group elements are demonstrated by Fig. 11a and c. The content

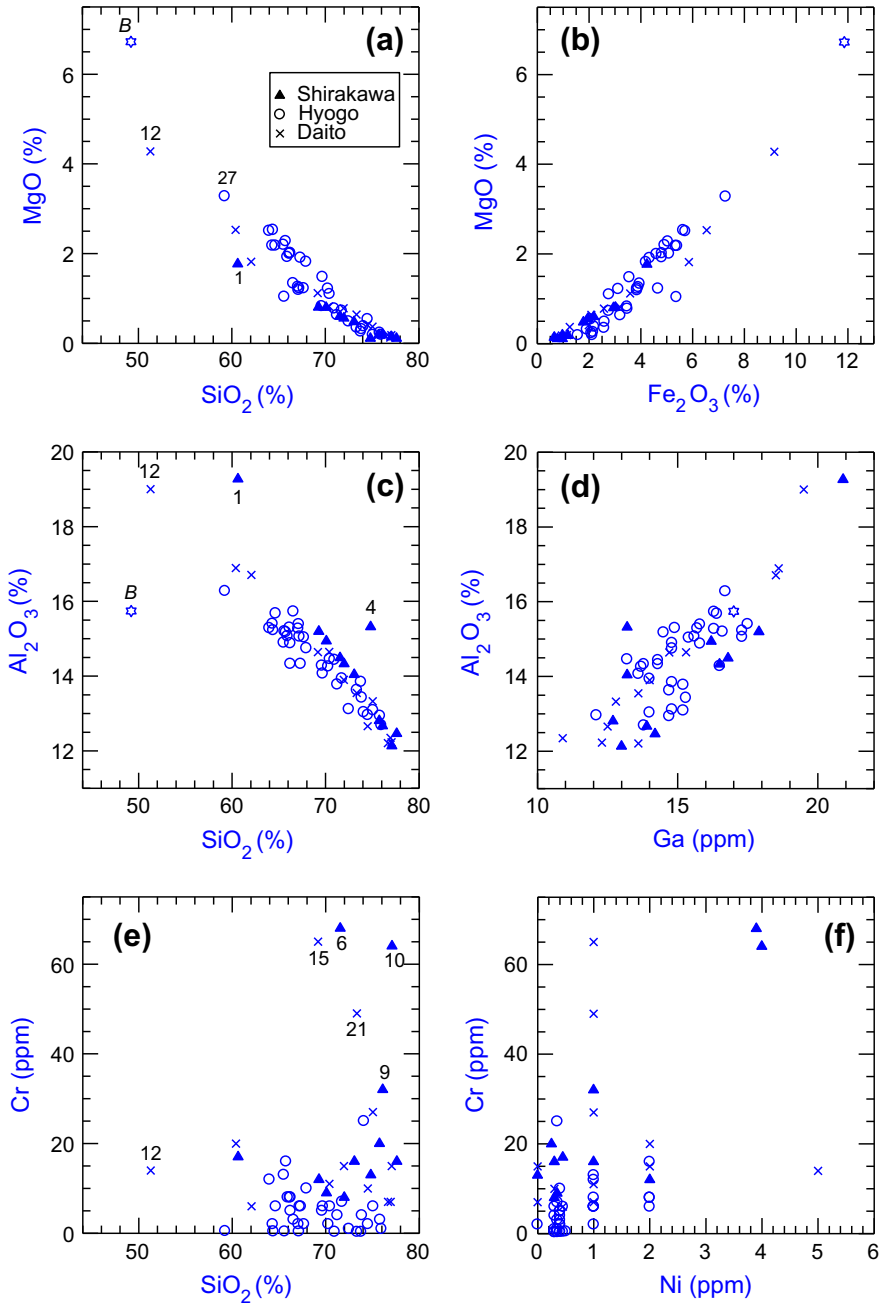

Fig. 10. *XY*-plots of the concentration data among selected mafic group elements, Cr and SiO_2 from Sanin belt. Sample symbols are the same as in Fig. 8.

of La diverges from the gabbroic sample 12 as SiO_2 content increases, and only a few samples fall below the dotted line (Fig. 11a); while Zr content diverges first, and then converges to low values below the dotted line by the fractional crystallization of zircon (Fig. 11c). Apparently no appreciable quantity of LREE carrying minerals such as apatite, allanite and monazite were produced to affect the removal of La and Ce for many Sanin samples. Certainly further study is warranted. Another element diverges from the gabbroic sample 12 with increasing SiO_2 content is the factor 2 element U (Fig. 11b), which correlates highly with Th and Rb (Fig. 9a). However, more than one half of samples fall below the dotted line and some are even $U_{sample} < U_{\#12}$, probably indicating effective removal of U^{4+} by minerals such as xenotime and coffinite etc. Daito samples 19, 20, 23, and Hyogo samples 1, 2, 7 are all high in both U and Si (Fig. 11b), suggesting an incompatible nature of U^{6+} in the relatively high oxygen fugacity magmas of those Sanin samples.

The factor analysis shows the high correlation between Zr and Na, which is confirmed by Fig. 11d. However, the Zr/Na ratio for Hyogo samples tend to be higher than that for Shirakawa and Daito samples (Fig. 11d). Apparently the fractional crystallization of Zr-bearing minerals (such as zircon) and Na-feldspar occurred roughly at the same stage of magmatic differentiation. At first glance, the variation patterns of Zr (Fig. 11c) and Sn (Fig. 11e) are quite different. However, Sn and Zr do correlate moderately when one looks at the Daito and Hyogo samples separately, but not Shirakawa samples (Fig. 11f). In magnetite series magma, Sn may exist as tetravalent Sn^{4+}. The ionic radius of Sn^{4+} (0.69 Å) is close to that of Zr^{4+} (0.72 Å), so Sn can be easily incorporated into Zr-bearing minerals. Further study on the mineral distribution

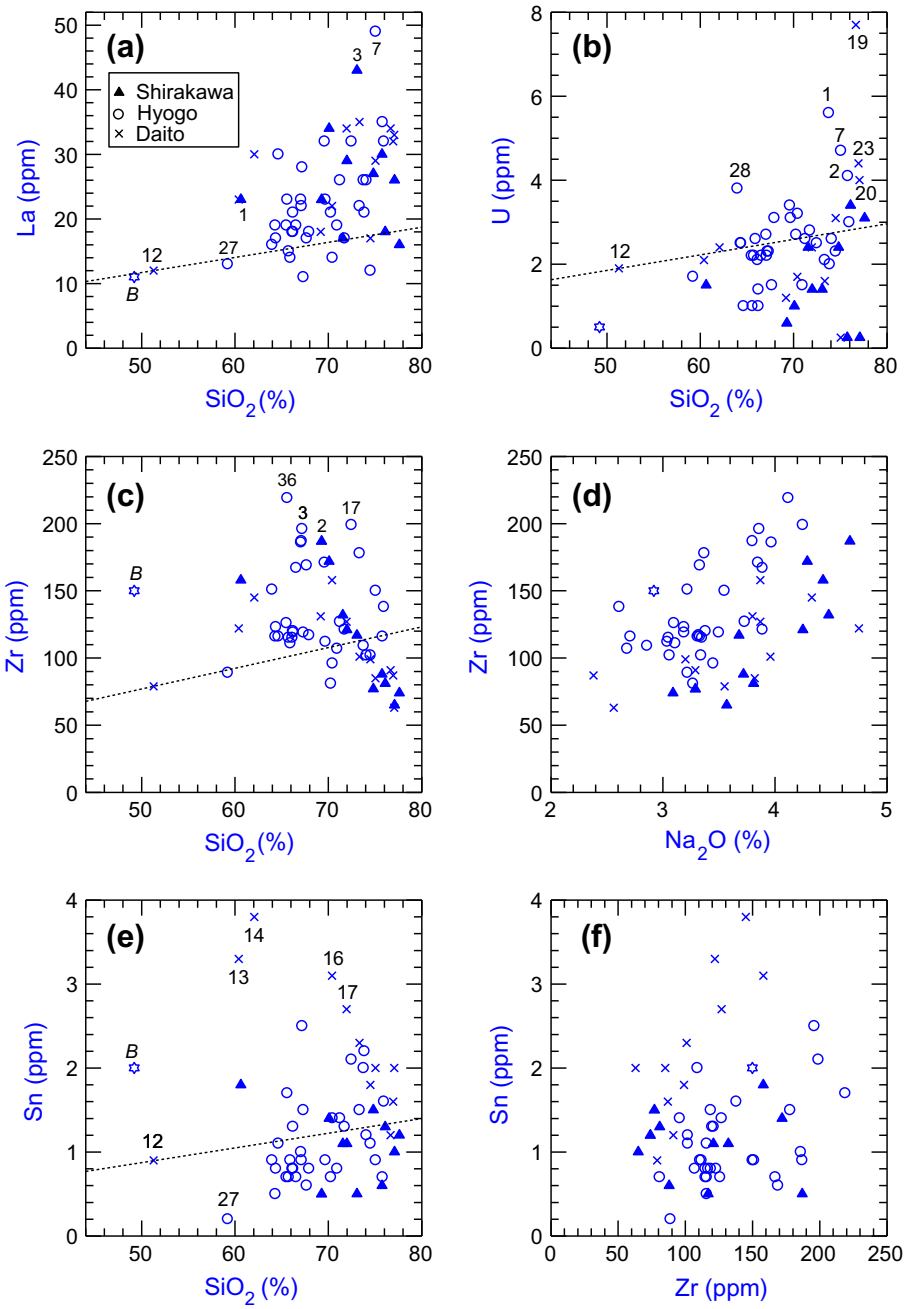

Fig. 11. *XY*-plots of the concentration data among La (LREE group), Zr (Y + Zr group), Mo, Sn, Na_2O, and SiO_2 from Sanin belt. The dotted straight line in each diagram represents the line connecting the origin and the data point of gabbroic Sanin sample 12 (primary magma). Sample symbols are the same as in Fig. 8.

coefficients of Sn and other trace metals in a zircon/matrix system will be useful.

Data points for the felsic group elements K, Rb, Tl, Pb and Th mostly fall above the dotted lines (Fig. 12a; Rb as an example), again indicating their high proportional gains relative to SiO_2. In the factor analysis, Cs does not correlate highly with any other elements, mainly caused by the systematically high Cs/Rb ratio in the Hyogo samples relative to Shirakawa and Daito samples (Fig. 12b). The Bi, Sb, and Se data have high analytical uncertainty but may belong to the felsic group because their concentrations tend to be high at high SiO_2 content (not shown).

Data points for W and Mo fall above and below the dotted line, and some are even less than the concentration values for the gabbroic sample 12 (Fig. 12c and e, respectively). W is nicely correlated with Pb (Fig. 12d) and with other felsic elements (Fig. 9a), as also is the case for the Ryoke + Sanyo belts samples. Even though Fig. 12c (SiO_2 versus W) and Fig. 12e (SiO_2 versus Mo) look similar at first glance, Mo does not correlate with W and any other elements (Fig. 12f). High Mo and Si contents in Daito samples 10, 13, 19, 21, and 23, and Hyogo samples 2 and 20 (Fig. 12e) may again suggest the conversion of Mo^{4+} into incompatible Mo^{6+} at relatively high oxygen fugacity conditions in the late stage of magmatic differentiation. The granitic plutons with high W and Mo contents could be the source rocks for the Mo and W ores in the Sanin belt. Mo and W ores in the Sanin belt occur mainly as molybdenite-quartz vein in granite and leucogranite; molybdenite–chlorite vein in aplitic granite; disseminated molybdenite in altered granite, aplite, and greisen; wolframite–molybdenite-quartz pipe in altered granite and pegmatite (Ishihara and Sasaki, 2002).

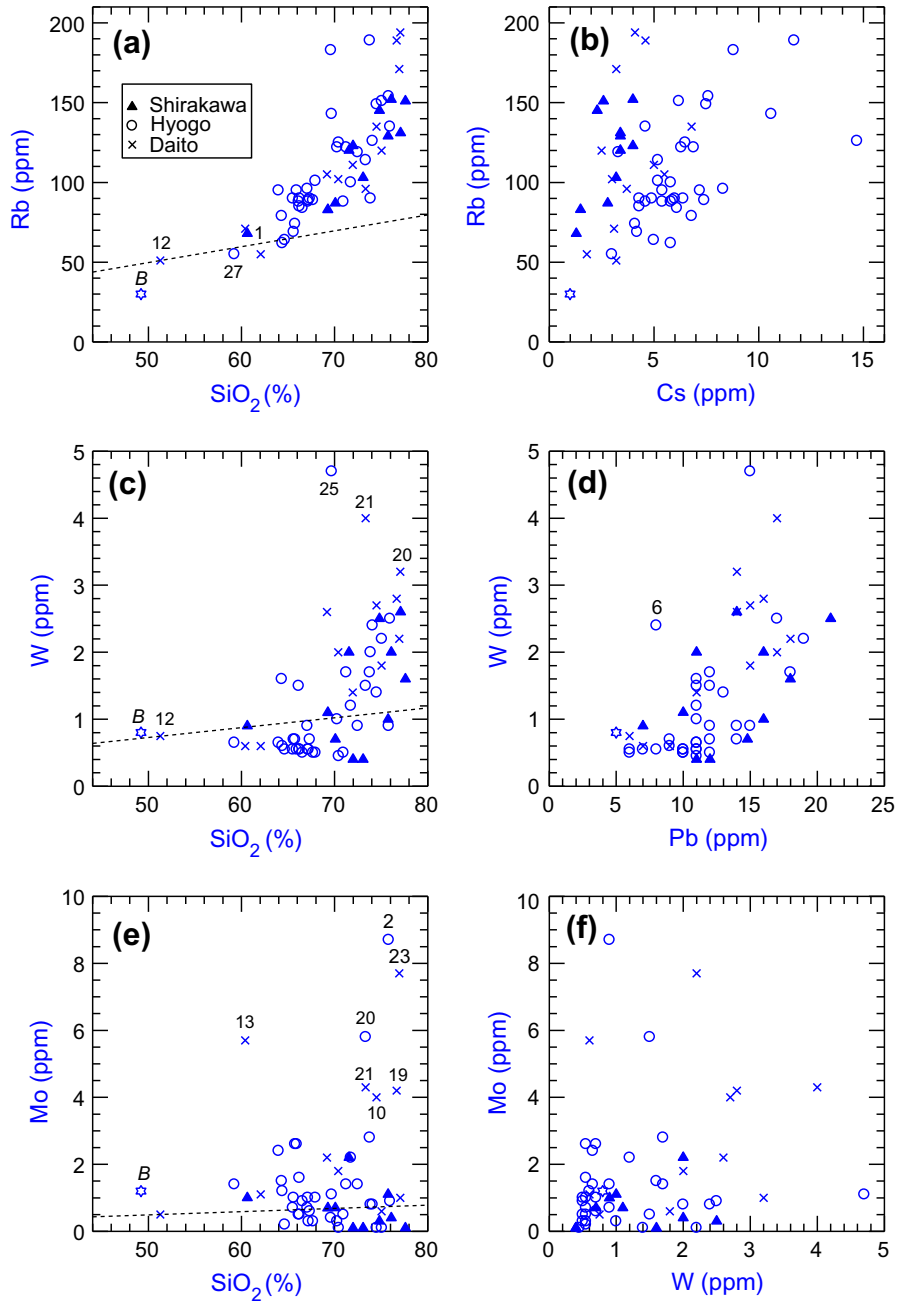

Fig. 12. *XY*-plots of the concentration data among selected felsic group elements, Mo, and SiO_2 from Sanin belt. Sample symbols are the same as in Fig. 8.

We have postulated two oxidation states for Cr(III, VI), Mo(IV, VI), Sn(II, IV), and U(IV, VI) to explain the change in their behaviors during the magmatic differentiation. However, it is quite uncertain as to under what redox conditions each element is transformed from a reducing state to oxidation state, or vice versa. Further study is needed.

4.3. Source rocks of primary magmas for the plutons in southwest Japan

As discussed earlier, the gabbroic Ryoke sample 45 and Sanin sample 12 may represent the overall primary magma compositions for the plutons in SW Japan. Fig. 13 shows the concentrations of various elements in these two gabbroic samples divided by those in the world average continental basalts (Li, 2000). Apparently their compositions mostly agree within a factor of two or better (within two dotted lines in Fig. 13). The obvious exceptions are Cu, Ni, and Cr, which are very much depleted in these two gabbroic samples as compared with the average continental basalt. The depletions may be attributed to the much earlier removal of crystallized forsteritic olivine and chrome spinel (for Ni and Cr), and sulfides (for Cu). Because the continental basalts are mainly differentiated from the fertile primitive mantle (PM; Hofmann, 1988), one may postulate that the primary basaltic magmas for the plutons in SW Japan were first produced by the partial melting of mantle wedge, whose composition is also similar to the fertile primitive mantle. Underplating of basaltic magmas beneath the continental crust might further facilitate the partial melting of the lower continental crusts. Because our samples were mainly collected for the W and Mo ores exploration, thus biased toward the

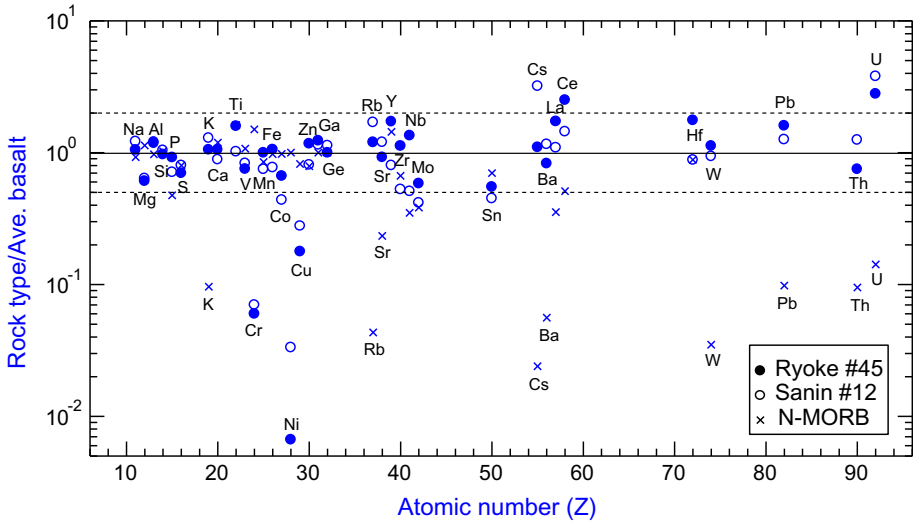

Fig. 13. Ratios of the concentration data between a given rock type (Ryoke sample 45, Sanin sample 12, and the average normal mid-ocean ridge basalts N-MORB) and the average continental basalts as a function of atomic number Z. The dotted lines represent a factor of two deviation from the continental basalt composition.

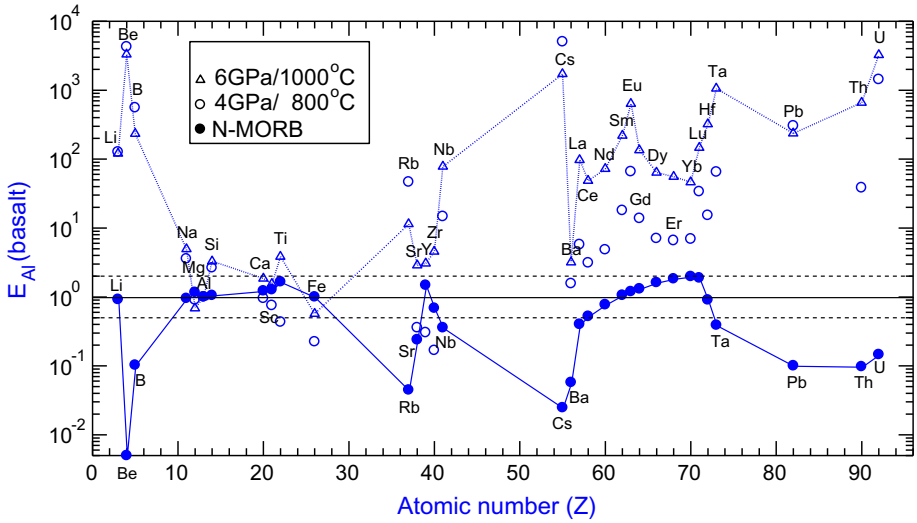

Fig. 14. Enrichment factors (normalized to Al and the average composition of the continental basalt as a reference) of various elements for the aqueous fluid (800 °C/4 GPa), supercritical liquid (100 °C/6 GPa; Kessel et al., 2005a, 2005b), and the average normal mid-ocean ridge basalts (N-MORB).

granitic plutons. Certainly we need to collect more samples from gabbroic plutons to ascertain the similarity in composition between the Japanese Arc gabbros and the average continental basalts.

In Fig. 13, the data for the normal mid-ocean ridge basalt (N-MORB; Li, 2000) are also given (as crosses). The elements K, Rb, Sr, Cs, Ba, La, Ce, W, Pb, Th, and U are all very much depleted in the N-MORB as compared with the average continental basalts and the gabbroic pluton samples. Therefore, the depleted upper mantle (DM), which is the source rock for N-MORB, cannot be the major source rock for the primary magmas of our selected plutonic samples. As discussed earlier, the basaltic oceanic crust (N-MORB) also cannot be the major source rocks because our selected granitic samples are neither adakites nor ocean ridge granites (Fig. 3g and h). Furthermore, the subducting oceanic basalts tend to become ecologites after dehydration at depth and be transported into the lower mantle (Iwamori, 2007; Kawakatsu and Watada, 2007). However, some granitoids from Tamba in the Sanyo belt are shown to be adakites (Kiji et al., 2000). A search for more adakites is warranted to gauge the extent of oceanic crust contribution to the plutons in SW Japan.

Another possible scenario is that the mantle wedge may have the composition of the depleted oceanic mantle (DM; Togashi et al., 2000); the primary magmas were produced by partial melting of the DM; and the depleted elements in the produced basaltic magmas (N-MORB) were replenished by the fluid, hydrous melt, and supercritical liquid liberated from the subducting oceanic crust (Kessel et al., 2005a, 2005b). According to the calculated enrichment factor E_{Al} (=$[X/Al]_{sample}/[X/Al]_{reference}$, where X and Al are the concentrations of elements X and Al, and the world average continent basalts is adopted as the reference; Fig. 14), the depleted elements such as B, Rb, Sr, Nb, Cs, Ba, La, Ce, Pb, Th, and U in the N-MORB can be replenished by the fluid (800 °C/4 GPa) and supercritical liquid (1000 °C/6 GPa) (Fig. 14). However, there are oversupplies of Li, Na, Si, and REE other than La and Ce from those liquids to the mixtures. If one can find some reasonable processes

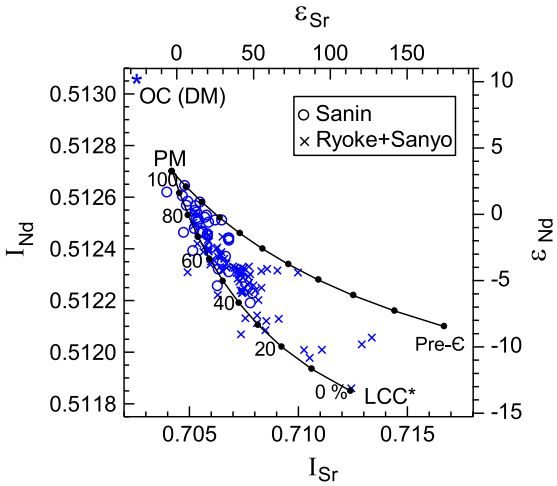

Fig. 15. Variation patterns of I_{Sr} (or ε_{Sr}) and I_{Nd} (or ε_{Nd}) values for the Sanin and Ryoke + Sanyo samples. See the text for model parameters used for the mixing curves among the fertile primitive mantle (PM), the least PM contaminated lower continental crust (LCC*), and the Precambrian metasediments (pre-Є). The star symbol is the oceanic crust (OC) or the depleted upper mantle (DM).

to remove those excess elements, the proposed scenario will become attractive. The partial melting of the mantle wedge with the DM composition would also contribute to the growth of the Japanese Arc. Certainly more detailed studies are needed.

Among the recent compilation of Sr and Nd isotope data for the granitic plutons from SW Japan (Jahn, 2010), there are 355 samples with age between 50 and 110 Ma. They have a mean age of 80 ± 11 Ma; the mean I_{Sr} (or ε_{Sr}) of 0.7072 ± 0.0018 (or 39 ± 26); and the mean I_{Nd} (or ε_{Nd}) of 0.51235 ± 0.00014 (or −3.7 ± 3.0). The plot of I_{Sr} versus I_{Nd} for those samples is shown in Fig. 15, which resembles Fig. 2c. The ε_{Sr} and ε_{Nd} scales in Fig. 15 are relative to the I_{Sr} and I_{Nd} values of the CHUR at 80 Ma ago. Because there are no data on the I_{Sr} and I_{Nd} values for the lower continental crust (LCC), we choose the Ryoke + Sanyo sample with the lowest I_{Nd} value as the end member of the least primitive-mantle-contaminated lower continental crust (LCC*). The mixing curve between the PM (fertile primitive mantle) and the LCC* end members (Fig. 15) is based on the assignment of the following parameters into the two end member mixing model of isotopic ratios (Faure and Mensing, 2005): I_{Sr} = 0.7042 and I_{Nd} = 0.51270 for PM; I_{Sr} = 0.7124 and I_{Nd} = 0.51185 for LCC*; Sr (PM)/Sr (LCC*) = 2.5; and Nd (PM)/Nd (LCC*) = 1. The mixing curve between PM and the Precambrian metasediments (pre-Є) is based on the additional assignment of I_{Sr} = 0.7167 and I_{Nd} = 0.51210 for pre-Є; Sr (PM)/Sr (pre-Є) = 2; and Nd (PM)/Nd (pre-Є) = 1, calculated back to 80 Ma ago (Kagami et al., 2006). The contribution of the PM to the average primary magmas for the Sanin samples is at least more than 70 and up to 100%. For the Ryoke + Sanyo samples, it is more than 50 ± 10% (Fig. 15). The rest is mainly contributed by the LCC, but the contribution from the pre-Є metasediments is always there and sometime becomes significantly large for Ryoke + Sanyo samples (Fig. 15). The protoliths of pre-Є metasediments may contain sufficient biogenic carbon and sulfur to cause the Ryoke + Sanyo belts to become relatively low in oxygen fugacity and $\delta^{34}S$ values as compared with the Sanin belt.

One may conclude that the Cretaceous–Paleogene plutons from SW Japan had contributed to the growth of continental crust with new, non-recycled materials during the Phanerozoic Eon (Nakajima et al., 2004). In contrast, Jahn (2010) proposed that the generation of granitoids in SW Japan was most likely dominated by the remelting of Precambrian crustal sources without much of later inputs from the upper mantle and oceanic crust. His conclusion is based on the calculated separation ages of granitoids from the mantle as obtained by the depleted mantle single-stage and 2-stage Sm–Nd models. However, as shown by Nakajima et al. (2004) and Kagami et al. (2006), I_{Sr} and I_{Nd} values for the Precambrian metasediments in SW Japan do not fall on the field for gabbroic and granitic plutons (Fig. 15). Moreover, any model, including the Sm–Nd models, always involves assumptions and uncertainties (DePaolo et al., 1991). The slight positive ε_{Nd} values for a few plutons from SW Japan (Fig. 15) may represent their innate property of the fertile primitive mantle underneath. However, one cannot rule out some transmission of isotopic signals from the oceanic crust (OC in Fig. 15 with $\varepsilon_{Sr} \approx -28$ and $\varepsilon_{Nd} \approx 10$; Wilson, 1989) to the fertile mantle wedge through the released liquids from subducted slabs. The mantle wedge with a depleted upper mantle (DM) composition also can provide the end member with $\varepsilon_{Sr} \approx -28$ and $\varepsilon_{Nd} \approx 10$.

5. Summary and conclusions

(1) The late Cretaceous–Paleogene plutons from SW Japan are separated into three major belts: the ore-barren Ryoke belt (110–70 Ma); W–Sn-ore-rich Sanyo belt (110–70 Ma); and Mo-ore-rich Sanin belt (85–30 Ma) (Fig. 1). The Ryoke + Sanyo rocks are characterized by the absence of magnetite and the Sanin rocks by the presence of magnetite. The former were formed under a lower oxygen fugacity condition than the latter. Our selected granitoid samples mostly belong to the class of sub-alkali, I-type, volcanic-arc, and non-adakite granites (Fig. 3).

(2) According to the factor analysis of the Ryoke + Sanyo chemical data, the elements can be separated into three major groups: mafic; LREE + Zr; and felsic groups (Fig. 4). Those groupings can be best explained by the fractional crystallization of primary magmas during magmatic differentiation. The mafic group elements crystallize and settle first, then, the LREE + Zr group, and then Na-feldspar. The felsic group elements are concentrated in the residual magmas. A few gabbroic samples are cumulates at the early stage of magmatic differentiation. Ryoke sample 45 may be representative of the overall primary magma composition in the Ryoke + Sanyo belts.

(3) The LREE + Zr group elements also include Ba and Hf in the Ryoke + Sanyo belts. Their concentrations increase first and then decrease with increasing SiO_2 content (Fig. 6a and c). The Zr/Hf ratio tends to decrease from Ryoke to Sanyo samples, and to the Sanyo leucogranite samples (Fig. 6d), indicating the progression of magmatic differentiation (Linnen and Keppler, 2002). Excluding a few high Mo Sanyo samples, Mo and Zr contents correlate nicely (Fig. 6f). The Mo/Zr ratio tends to be higher in the Sanyo samples than in the Ryoke samples. The high Mo and Si contents in a few Sanyo samples may indicate that the zircon-compatible Mo^{4+} were converted into incompatible Mo^{6+} under a relatively high oxygen fugacity condition in the magmas of those samples at the late stage of magmatic differentiation.

(4) W and Sn belong to the felsic group elements and their concentrations are high in the granitic Sanyo samples, especially in leucogranites (Fig. 7d). Therefore, the granitic plutons from the Sanyo belt are ideal source rocks for the associated W–Sn ores. In contrast, the granitic Ryoke samples have the lowest Mo content due to its removal by zircon (Fig. 6e), and low in W and Sn content due to the lack of the advanced magmatic differentiation stage, which would produce W + Sn rich magma similar to leucogranite (Figs. 4c and 7d). Therefore the Ryoke belt ends up as ore-barren.

(5) The elements in Sanin samples also separate into the mafic and felsic groups. However, Cr and Ni no longer belong to the mafic group, nor Sn and Y to the felsic group. The LREE + Zr group in Ryoke + Sanyo belts split into two independent Y + Zr group and LREE group in the Sanin belt (Fig. 9). The Y + Zr group also includes Ba, Hf, Nb, and Ta. The breakdown in the correlation between Cr and Ni (Fig. 10f) may result from the conversion of highly compatible Cr^{3+} to incompatible Cr^{6+} under a relatively high oxygen fugacity condition at the late stage of magmatic differentiation.

(6) Some Sanin samples are high in both Mo and Si (Fig. 12e), but Mo does not correlate with any other elements, again suggesting the conversion of the zircon-compatible Mo^{4+} into incompatible Mo^{6+} in the magmas of those samples at the late stage. Sn in the Sanin samples no longer correlates with W and other felsic group elements, but it does correlate with Zr separately for the Daito and Hyogo samples (Fig. 11f). In the magnetite series magma, Sn may exist as tetravalent Sn^{4+}, whose ionic radius is close to Zr^{4+}, and can be easily incorporated into Zr-bearing minerals.

(7) The plots of the logarithmic concentration of Th versus that of X (elements other than Th) from each ore belt (Ryoke, Sanyo and Sanin) follow more or less the Rayleigh fractional crystallization model (Fig. 8).

(8) The gabbroic Ryoke sample 45 and Sanin sample 12 may represent the overall primary magma compositions for the plutons in SW Japan. Their compositions agree with the world average continental basalts within a factor of two or better (Fig. 13). The obvious exceptions are Cu, Ni, and Cr, which were probably left behind as sulfides during the partial melting. The source rocks for the primary magmas of the plutons include mainly the fertile primitive mantle, the lower continental crust, and the Precambrain metasediments. The oceanic crust and depleted upper mantle (DM) as possible source rocks for the primary magmas needs further study (Fig. 14).

(9) The Ryoke + Sanyo samples tend to have relatively high $\delta^{18}O$ and ε_{Sr}, and low $\delta^{34}S$ and ε_{Nd} values as compared to Sanin (Fig. 2) due to the incorporation of the lower crust materials and the Precambrian metasediments (Fig. 15). The protoliths of Precambrian metasediments may contain sufficient biogenic carbon and sulfur to cause the Ryoke + Sanyo belts to become relatively low in oxygen fugacity and $\delta^{34}S$ values. The calculated contribution of the lower continental crust (LCC) to Sanin basaltic magmas is near zero to at most 30%, and ~50% for the majority of Ryoke + Sanyo basaltic magmas. The remainder is mainly contributed by the fertile primitive mantle (PM). Therefore, the Cretaceous–Paleogene plutons from SW Japan have contributed to the growth of new, non-recycled component in the continental crust during the Phanerozoic.

Acknowledgements

Constructive comments by Dr. Tony Kemp and one anonymous reviewer are most helpful. Ms. May Izumi provided editorial assistances. SOEST contribution # 8922.

References

Chappell, B.W., White, A.J.R., 1974. Two contrasting granite types. Pacific Geol. 8, 173–174.
Chappell, B.W., White, A.J.R., 2001. Two contrasting granite types: 25 years later. Aust. J. Earth Sci. 48, 489–499.
Cooley, W.W., Lohnes, P.R., 1971. Multivariate Data Analysis. Wiley and Sons, New York.
Davis, J.C., 1973. Statistics and Data Analysis in Geology. Wiley, New York.
DePaolo, D.J., Linn, A.M., Schubert, G., 1991. The continental crustal age distribution: methods of determining mantle separation ages from Sm–Nd isotopic data and application to the southwestern United States. J. Geophys. Res. 96 (B2), 2071–2088.
Drummond, M.S., Defant, M.J., 1990. A model of trondhjenite–tonalite–dacite genesis and crustal growth via slab melting: Archean to modern comparison. J. Geophys. Res. 95 (B13), 21503–21521.
Faure, G., Mensing, T.M., 2005. Isotopes: Principles and Applications, third ed. Wiley and Sons, New York.
Heckel, J., Ryon, R.W., 2002. Polarized beam Xray fluorescence analysis. In: Van Grieken, R., Markowicz, A.A. (Eds.), Handbook of X-ray Spectrometry, second ed. Marcel Dekker, Inc..
Hofmann, A.W., 1988. Chemical differentiation of the Earth: the relationship between mantle, continental crust, and oceanic crust. Earth Planet. Sci. Lett. 90, 297–314.
Ishihara, S., 1977. The magnetite-series and ilmenite-series granitic rocks. Min. Geol. 27, 293–305.
Ishihara, S., 1978. Metallogenisis of the Japanese Island Arc system. J. Geol. Soc. London 135, 389–406.
Ishihara, S., 2002a. Chemical characteristics of the mineralized granitoids (I): Mo and W provinces of the Inner Zone of Southwest Japan. Bull. Geol. Surv. Jpn 53, 657–672 (in Japanese with English abstract).
Ishihara, S., 2002b. Chemical characteristics of the mineralized granitoids (II): polymetallic province of the west-central Hyogo Prefecture, Japan. Bull. Geol. Surv. Jpn 53, 673–688 (in Japanese with English abstract).
Ishihara, S., Matsuhisa, H., 2002. Oxygen isotopic constrains on the genesis of the Cretaceous–Paleogene granitoids in the Inner Zone of Southwest Japan. Bull. Geol. Surv. Jpn 54, 421–438.
Ishihara, S., Sasaki, A., 2002. Paired sulfur isotopic belts: late Cretaceous–Paleogene ore deposits of southwest Japan. Bull. Geol. Surv. Jpn 53, 461–477.
Ishihara, S., 2003. Chemical contrast of the late Cretaceous granitoids of the Sanyo and Ryoke Belts, Southwest Japan: Okayama–Kagawa Transect. Bull. Geol. Surv. Jpn 53, 96–116.
Ishihara, S., Chappell, B.W., 2007. Chemical compositions of the late Cretaceous Ryoke granitoids of the Chubu district, central Japan – Revisited. Bull. Geol. Surv. Jpn 58, 323–350.
Ishihara, S., Chappell, B.W., 2008. Chemical compositions of the Paleogene granitoids of eastern Shimane prefecture, Sanin district, southwest Japan. Bull. Geol. Surv. Jpn 59, 225–254.
Isozaki, Y., 1996. Constrasting two types of orogen in Permo-Triassic Japan: accretionary versus collisional. The Island Arc 6, 2–24.
Isozaki, Y., Aoki, K., Nakama, T., Yanai, S., 2010. New insight into a subduction-related orogen: a reappraisal of the geotectonic framework and evolution of the Japanese Islands. Gondwana Res. 18, 82–105.
Iwamori, H., 2007. Transportation of H_2O beneath the Japan arcs and its implications for global water circulation. Chem. Geol. 239, 182–198.
Jahn, B.M., 2010. Accretionary orogen and evolution of the Japanese islands: implications from a Sr–Nd isotopic study of the Phanerozoic grantoids from SW Japan. Am. J. Sci. 310, 1210–1249.
Kagami, H., Iizumi, S., Tanosho, Y., Owada, M., 1992. Spatial variation of Sr and Nd isotope ratios of Cretaceous–Paleogene granitoid rock, Southwest Japan Arc. Contrib. Min. Petrol. 112, 165–177.
Kagami, H., Kawano, Y., Akiyama, M., Ikawa, T., Imaoka, T., Ishioka, J., Toyoshima, T., Hamamoto, T., Hayasaka, Y., Ikeda, Y., Yuhara, M., Tainosho, Y., 2006. Provenance of Paleozoic–Mesozoic sedimentary rocks in the Inner Zone of Southwest Japan: an evaluation based on Nd model ages. Gondwana Res. 9, 142–151.
Kawakatsu, H., Watada, S., 2007. Seismic evidence for deep-water transportation in the mantle. Science 316, 1468–1471.
Kanaya, H., Ishihara, S., 1973. Regional variation of magnetic susceptibility of the granitic rocks in Japan. Jpn. Assoc. Miner. Petrol. Econ. Geol. 68, 211–224 (in Japanese with English abstract).
Kessel, R., Schmidt, M.W., Ulmer, P., Pettk, T., 2005a. Trace element signature of subduction-zone fluids, melts and supercritical liquids at 120–180 km depth. Nature 437, 724–727.
Kessel, R., Ulmer, P., Pettke, T., Schmidt, M.W., Thompson, A.B., 2005b. The water–basalt system at 4 to 6 GPa: phase relations and second critical endpoint in a K-free eclogite at 700 to 1400 °C. Earth Planet. Sci. Lett. 237, 873–892.
Kiji, M., Ozawa, H., Murata, M., 2000. Cretaceous adakitic Tamba granitoids in northern Kyoto, Sanyo belt, southwest Japan. Rock Mineral Sci. 29, 136–149 (in Japanese with English abstract).
Li, Y.H., 2000. A Compendium of Geochemistry: From Solar Nebula to the Human Brain. Princeton University Press, Princeton.
Linnen, R.L., Keppler, H., 2002. Melt composition control of Zr/Hf fractionation in magmatic processes. Geochim. Cosmochim. Acta 66, 3293–3301.
Miyashiro, A., 1974. Volcanic rock series in island arcs and active continental margin. Am. J. Sci. 274, 321–355.
Maruyama, S., 1997. Pacific-type orogeny revisited: miyashiro-type orogeny proposed. The Island Arc 6, 91–120.
Nakajima, T., Kamiyama, H., Williams, I.S., Tani, K., 2004. Mafic rocks from the Ryoke belt, southwest Japan: implications for Cretaceous Ryoke/Sanyo granitic magma genesis. Trans. Royal Soc. Edinburgh: Earth Sci. 95, 249–263.

Pearce, J.A., Harris, N.B.W., Tindle, A.G., 1984. Trace elements discrimination diagrams for the tectonic interpretation of granitic rocks. J. Petro. 25, 956–983.
Rudnick, R.L., 1995. Making continental crust. Nature 378, 571–578.
Sasaki, A., Ishihara, S., 1979. Sulfur isotopic composition of the magnetite-series and ilmenite-series granitoids in Japan. Contrib. Petrol. Mineral. 68, 107–115.
Spandler, C., Mavrogens, J., Hermann, J., 2007. Experimental constraints on element mobility from subducted sediments using high-P synthetic fluid/melt inclusions. Chem. Geol. 239, 228–249.
Togashi, S., Imai, N., Okuyama-Kusunose, Y., Tanaka, T., Okai, T., Koma, T., Murata, Y., 2000. Young upper crustal chemical composition of the orogenic Japan Arc. Geochem. Geophys. Geosyst. 1, Paper Number 2000GC000083.
Urabe, T., 1985. Aluminous granite as a source magma of hydrothermal ore deposits: an experimental study. Econ. Geol. 80, 148–157.
Wilson, M., 1989. Igneous Petrogenesis: A Global Tectonic Approach. Unwin Hyman, London.